

# Feature extraction from spike trains with Bayesian binning:

'Latency is where the signal starts'

Dominik Endres and Mike Oram

Received: 13 November 2008 / Revised: 2 March 2009 / Accepted: 14 April 2009

**Abstract** The peristimulus time histogram (PSTH) and its more continuous cousin, the spike density function (SDF) are staples in the analytic toolkit of neurophysiologists. The former is usually obtained by binning spike trains, whereas the standard method for the latter is smoothing with a Gaussian kernel. Selection of a bin width or a kernel size is often done in a relatively arbitrary fashion, even though there have been recent attempts to remedy this situation (DiMatteo et al 2001; Shimazaki and Shinomoto 2007c,b,a; Cunningham et al 2008). We develop an exact Bayesian, generative model approach to estimating PSTHs. Advantages of our scheme include automatic complexity control and error bars on its predictions. We show how to perform feature extraction on spike trains in a principled way, exemplified through latency and firing rate posterior distribution evaluations on repeated and single trial data. We also demonstrate using both simulated and real neuronal data that our approach provides a more accurate estimates of the PSTH and the latency than current competing methods. We employ the posterior distributions for an information theoretic analysis of the neural code comprised of latency and firing rate of neurons in high-level visual area STSa. A software implementation of our method is available at the machine learning open source software repository ([www.mloss.org](http://www.mloss.org), project 'binsdfc').

**Keywords** spike train analysis · Bayesian methods · response latency · PSTH · SDF · information theory

## 1 Introduction

Plotting a peristimulus time histogram (PSTH), or a spike density function (SDF), from spiketrains evoked by and aligned

to the onset of a stimulus is often one of the first steps in the analysis of neurophysiological data. It is an easy way of visualising certain characteristics of the neural response, such as instantaneous firing rates (or firing probabilities), latencies and response offsets. These measures also implicitly represent a model of the neuron's response as a function of time and are important parts of their functional description. Yet PSTHs are frequently constructed in an unsystematic manner, e.g. the choice of time bin size is driven by result expectations as much as by the data. Recently, there have been more principled approaches to the problem of determining the appropriate temporal resolution (Shimazaki and Shinomoto 2007c,b,a).

We recently developed an exact Bayesian, generative model approach to estimating PSTH/SDFs (Endres et al 2008). Our model encodes a spike generator described by an inhomogeneous Bernoulli process with piecewise constant (in time) firing probabilities. We demonstrated that relevant marginal distributions, e.g. the posterior distribution of the number of bins, can be evaluated from the full posterior distribution over the model parameters efficiently, i.e. in polynomial time. Extending earlier dynamic programming schemes (Endres and Földiák 2005), we also showed that expected values, such as the predictive firing rate and its standard error, are computable with at most cubic effort.

Here we extend the performance comparisons in (Endres et al 2008) and illustrate the usefulness of our method. We also demonstrate how to use our Bayesian approach for principled feature extraction from spike trains. Specifically we examine latencies and firing rates, since previous studies (Richmond and Optican 1987b; Tovee et al 1993) indicate that much of the stimulus-related information carried by neurons is contained in these measures (see (Oram et al 2002) for a review). We give a 'minimal' definition of latency and show how the latency posterior distribution and the firing rate posterior density can be evaluated. These posteriors are

D. Endres, M. Oram  
School of Psychology, University of St. Andrews, KY16 9JP, UK  
E-mail: {dme2,mwo}@st-andrews.ac.uk

then employed for an information theoretic analysis of the neural code comprised of latency and firing rate. Note that we do in no way claim that a PSTH is a complete generative description of spiking neurons. We are merely concerned with inferring that part of the generative process which can be described by a PSTH in a Bayes-optimal way. This paper tries to appeal to computational neuroscientists and neurophysiologists alike. While the former require sound derivations to accept a method’s validity, the latter need to be convinced of a method’s superiority through demonstrations if they are to adopt it. We attempt to present a balanced mix of both.

## 2 The model

### 2.1 Traditional approaches

The traditional approaches to estimating firing probabilities or firing rates from neurophysiological data can roughly be divided into two classes: binning and smoothing. The former yields PSTHs, whereas the latter produces SDFs (Richmond and C 1987a). Both are instances of regularisation procedures, which try to deal with the ubiquitous noise and data scarcity by making various implicit assumptions. From a generative model perspective, binning basically presupposes that the firing probabilities are constant within each bin, whereas smoothing imposes the prior belief that high-frequency fluctuations are mostly noise. Whether these assumptions are correct can not be decided a priori, but must be evaluated by comparing the predictive performances of all models in question on real neurophysiological data (see section 3.4).

An intuitive understanding of the relative merits and drawbacks of these two approaches can be obtained from fig.1: panel A shows a rastergram of 32 spiketrains recorded from an STSa neuron in response to a stimulus. Each tick represents a spike, with the spiketrains (rows) aligned to stimulus onset. Panel B shows a PSTH with a fixed bin duration, optimised for the data by the method described in (Shimazaki and Shinomoto 2007c,b). While a bin PSTH could in principle model sharp transients, the location of the bin boundaries are determined by the constant binwidth. Therefore, the precise onset of the transient is often not captured well. In addition, the constant bin duration also forces this method to put many bins into time intervals where the spike-trains appears relatively constant, e.g. in [200ms,400ms]. Panel C depicts the SDF obtained by smoothing these spike-trains with a Gaussian kernel of 10ms width. Compared to the rastergram, high frequency fluctuation in the spiketrains is reduced to some degree, as can be seen e.g. in the interval [200ms,400ms]. However, the sharp transient at  $\approx 100$ ms (indicated by the dashed vertical line across panels B-D), becomes blurred. Thus, relevant timing information might be lost.

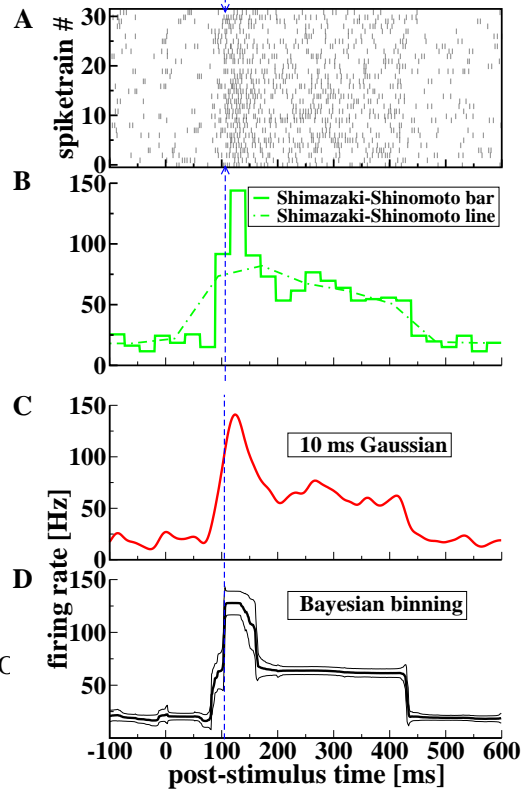


**Fig. 1** Predicting a PSTH/SDF with 3 different methods. *A*: the dataset used in this comparison consisted of 32 spiketrains recorded from a STSa neuron. This neuron was chosen for its clear response profile. Each tick mark represents a spike. *B*: bar PSTH (solid line), optimal binsize  $\approx 26$ ms, and line PSTH (dashed line), optimal binsize  $\approx 78$ ms, computed by the methods described in (Shimazaki and Shinomoto 2007c,b). *C*: SDF obtained by smoothing the spike trains with a 10ms Gaussian kernel. *D*: PSTH inferred with our Bayesian binning method. The thick line represents the predictive firing rate, the thin lines show the predictive firing rate  $\pm 1$  standard deviation. Models with  $4 \leq M \leq 13$  were included on a risk level of  $\alpha = 0.1$  (see eqn.(17)). The vertical dashed line indicates the mode of the latency posterior (see section 4.1 and fig.5).

Finally, both binning and smoothing are often employed to compute point estimates of the instantaneous firing rate. Given the typically small sample sizes in neurophysiological experiments, reliable point estimates are hard to obtain, and measures of posterior uncertainty and variability, both between and within trials, should be a part of the estimation procedure. Our Bayesian binning method (fig.1, D) achieves this goal.

### 2.2 Bayesian binning

We propose a compromise between binning and smoothing to deal with the problems described in the previous section: keep the bins to allow for rapid changes in the instantaneous firing rate, but allow for varying bin durations. This enables

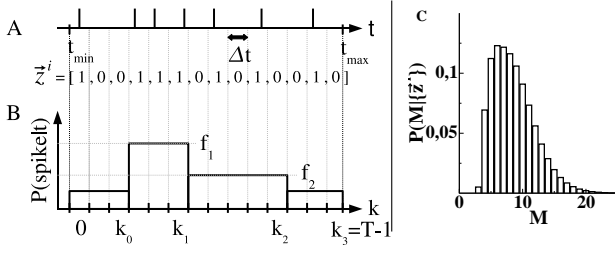


**Fig. 2** A: A spike train, recorded between times  $t_{min}$  and  $t_{max}$  is represented by a binary vector  $\mathbf{z}^i$ . B: The time span between  $t_{min}$  and  $t_{max}$  is discretised into  $T$  intervals of duration  $\Delta t = (t_{max} - t_{min})/T$ , such that interval  $k$  lasts from  $k \times \Delta t + t_{min}$  to  $(k+1) \times \Delta t + t_{min}$ .  $\Delta t$  is chosen such that at most one spike is observed per  $\Delta t$  interval for any given spike train. Then, we model the firing probabilities  $P(\text{spike}|t)$  by  $M+1 = 4$  contiguous, non-overlapping bins ( $M$  is the number of bin boundaries inside the time span  $[t_{min}, t_{max}]$ ), having inclusive upper boundaries  $k_m$  and  $P(\text{spike}|t \in (t_{min} + \Delta t(k_{m-1} + 1), t_{min} + \Delta t(k_m + 1))) = f_m$ . C: model posterior  $P(M|\{\mathbf{z}^i\})$  (see eqn.(16)) computed from the data shown in fig.1. The shape is fairly typical for model posteriors computed from the neural data used in this paper: a sharp rise at a moderately low  $M$  followed by a maximum (here at  $M = 6$ ) and an approximately exponential decay. Even though a maximum  $M$  of 699 would have been possible,  $P(M > 23|\{\mathbf{z}^i\}) < 0.001$ . Thus, we can accelerate the averaging process for quantities of interest (e.g. the predictive firing rate) by choosing a moderately small maximum  $M$ . For details, see text.

us to put the bin boundaries at only those time points where the changes in firing rate happen. As a consequence, time intervals in which the firing rate does not change can now be modelled by one (or a few) bins, which reduces the risk of overfitting noise. Uncertainties and variabilities will be computed in an exact Bayesian fashion. The resultant expected firing rates (complete with their uncertainties) will therefore have a more continuous appearance, similar to the results yielded by a smoothing technique.

Details of the formal model have been described in (Endres et al. 2008). Briefly, we model a PSTH on  $[t_{min}, t_{max}]$  discretised into  $T$  contiguous intervals of duration  $\Delta t = (t_{max} - t_{min})/T$  (see fig.2, A and B). We select a discretisation fine enough (here 1ms) so that we will not observe more than one spike in a  $\Delta t$  interval for any given spike train. Spike train  $i$  can then be represented by a binary vector  $\mathbf{z}^i$  of dimensionality  $T$ . We model the PSTH by  $M+1$  contiguous, non-overlapping bins having inclusive upper boundaries  $k_m$ , within which the firing probability  $f_m = P(\text{spike}|t \in (t_{min} + \Delta t(k_{m-1} + 1), t_{min} + \Delta t(k_m + 1)))$  is constant. Importantly, the bin size (distance between bin boundaries) is not fixed *a priori* but can vary depending on the observed data. The relationship between the firing probabilities  $f_m$  and the instantaneous firing rates is given by

$$\text{firing rate} = \frac{f_m}{\Delta t}. \quad (1)$$

$M$  is the number of bin boundaries inside  $[t_{min}, t_{max}]$ . The probability of a spike train  $\mathbf{z}^i$  of independent spikes/gaps is then

$$P(\mathbf{z}^i|\{f_m\}, \{k_m\}, M) = \prod_{m=0}^M f_m^{s(\mathbf{z}^i, m)} (1 - f_m)^{g(\mathbf{z}^i, m)} \quad (2)$$

where  $s(\mathbf{z}^i, m)$  is the number of spikes and  $g(\mathbf{z}^i, m)$  is the number of non-spikes, or gaps in spiketrain  $\mathbf{z}^i$  in bin  $m$ , i.e. between intervals  $k_{m-1} + 1$  and  $k_m$  (both inclusive). In other words, we model the spiketrains by an inhomogeneous Bernoulli process with piecewise constant probabilities. We also define  $k_{-1} = -1$  and  $k_M = T - 1$ . Note that there is no binomial factor associated with the contribution of each bin, because we do *not* want to ignore the spike timing information within the bins, but rather, we try to build a simplified generative model of the spike train. Therefore, the probability of a (multi)set of spiketrains  $\{\mathbf{z}^i\} = \{z_1, \dots, z_N\}$ , assuming independent generation, is

$$\begin{aligned} P(\{\mathbf{z}^i\}|\{f_m\}, \{k_m\}, M) &= \prod_{i=1}^N \prod_{m=0}^M f_m^{s(\mathbf{z}^i, m)} (1 - f_m)^{g(\mathbf{z}^i, m)} \\ &= \prod_{m=0}^M f_m^{s(\{\mathbf{z}^i\}, m)} (1 - f_m)^{g(\{\mathbf{z}^i\}, m)} \end{aligned} \quad (3)$$

where  $s(\{\mathbf{z}^i\}, m) = \sum_{i=1}^N s(\mathbf{z}^i, m)$  and  $g(\{\mathbf{z}^i\}, m) = \sum_{i=1}^N g(\mathbf{z}^i, m)$ .

### 2.3 The priors

We make a non-informative prior assumption for the joint prior of the firing probabilities  $\{f_m\}$  and the bin boundaries  $\{k_m\}$  given the total number of bin boundaries  $M$ , namely

$$p(\{f_m\}, \{k_m\}|M) = p(\{f_m\}|M)P(\{k_m\}|M). \quad (4)$$

i.e. we have no a priori preferences for the firing rates based on the bin boundary positions. Note that the prior of the  $f_m$ , being continuous model parameters, is a density. Given the form of eqn.(2) and the constraint  $f_m \in [0, 1]$ , it is natural to choose a conjugate prior

$$p(\{f_m\}|M) = \prod_{m=0}^M B(f_m; \sigma_m, \gamma_m). \quad (5)$$

The Beta density is defined in the usual way (see e.g. (Berger 1985)):

$$B(p; \sigma, \gamma) = \frac{\Gamma(\sigma + \gamma)}{\Gamma(\sigma)\Gamma(\gamma)} p^{\sigma-1} (1-p)^{\gamma-1}. \quad (6)$$

There are only finitely many configurations of the  $k_m$ . Assuming we have no preferences for any of them, the prior for the bin boundaries becomes

$$P(\{k_m\}|M) = \frac{1}{\binom{T-1}{M}}. \quad (7)$$

where the denominator is just the number of possibilities in which  $M$  ordered bin boundaries can be distributed across  $T - 1$  places (bin boundary  $M$  always occupies position  $T - 1$ , see fig.2, B, hence there are only  $T - 1$  positions left).

## 2.4 Computing the evidence and other posterior expectations

To calculate quantities of interest for a given number of bin boundaries  $M$  and a set of spiketrains  $\{\mathbf{z}^i\}$ , e.g. predicted firing probabilities, their variances and expected bin boundary positions, we need to average the quantity of interest over the posterior of the firing rates in the bins  $\{f_m\}$  and the bin boundaries  $\{k_m\}$ :

$$P(\{f_m\}, \{k_m\} | M, \{\mathbf{z}^i\}) = \frac{P(\{\mathbf{z}^i\}, \{f_m\}, \{k_m\} | M)}{P(\{\mathbf{z}^i\} | M)} \quad (8)$$

which requires the evaluation of the evidence, or marginal likelihood of a model with  $M$  bins:

$$P(\{\mathbf{z}^i\} | M) = \sum_{k_{M-1}=M-1}^{T-2} \sum_{k_{M-2}=M-2}^{k_{M-1}-1} \dots \dots \sum_{k_0=0}^{k_1-1} P(\{\mathbf{z}^i\} | \{k_m\}, M) P(\{k_m\} | M) \quad (9)$$

where the summation boundaries are chosen such that the bins are non-overlapping and contiguous and

$$P(\{\mathbf{z}^i\} | \{k_m\}, M) = \int_0^1 d\{f_m\} P(\{\mathbf{z}^i\} | \{f_m\}, \{k_m\}, M) P(\{f_m\} | M). \quad (10)$$

with

$$\int_0^1 d\{f_m\} = \int_0^1 df_0 \int_0^1 df_1 \dots \int_0^1 df_M. \quad (11)$$

Computing the sums in eqn.(9) might seem difficult.  $M$  sums over  $O(T)$  summands suggest a computational complexity of  $O(T^M)$ , which is impractical. To appreciate why, let's consider an example: In a typical neurophysiological scenario, we might want to estimate the PSTH in a  $T = 700$ ms time window with  $\Delta t = 1$ ms. If we tried to model this distribution by  $M + 1 = 11$  bins, we would have to check  $\binom{699}{10}$  configurations, i.e. the number of possibilities to distribute 10 ordered bin boundaries across 699 places. This is  $> 10^{21}$ . Even if we checked 10 configurations per microsecond, we would take more than 20 million years to finish.

However, we can expedite this process. As previously demonstrated (Endres et al 2008), using dynamic programming the computational complexity can be reduced to  $O(MT^2)$ . In the above example, the time to compute the evidence reduces to  $\approx 0.5$  s, which is fast enough to be useful. We give a description of the algorithm in appendix A. This algorithm is also the basis for the latency calculations in section 4.1.

Posterior expectations can be evaluated in a similar fashion. For example, given the model parameters  $\{k_m\}, \{f_m\}$  and  $M$ , the predictive firing probability at time index  $t$  can formally be written as

$$P(\text{spike} | t, \{f_m\}, \{k_m\}, M) = \sum_{m=0}^M f_m \mathcal{I}(t \in \{k_{m-1} + 1, k_m\}) \quad (12)$$

where the indicator function  $\mathcal{I}(x) = 1$  iff  $x$  is true and 0 otherwise. Thus, the sum will have exactly one nonzero contribution from that bin which contains  $t$ . Multiplying the r.h.s. of eqn.(12) with the r.h.s. eqn.(8) and marginalising  $\{f_m\}$  and  $\{k_m\}$  yields the predictive firing probability at  $t$  given  $M$  and the data  $\{\mathbf{z}^i\}$ :

$$\langle P(\text{spike} | t) \rangle \quad (13)$$

where  $\langle \dots \rangle$  denotes a posterior expectation. The necessary summations/integrations can be done by a modified version of the algorithm described in appendix A: since eqn.(12) puts a factor  $f_m$  into the bin which contains  $t$ , we only need to add an 'extra' spike in this bin in eqn.(A-5), run the algorithm and divide the result by the evidence to obtain the predictive firing probability.

To compute the standard deviation of the firing probability, we need the posterior expectation of

$$P^2(\text{spike} | t, \{f_m\}, \{k_m\}, M) = \sum_{m=0}^M f_m^2 \mathcal{I}(t \in \{k_{m-1} + 1, k_m\}) \quad (14)$$

The factor  $f_m^2$  amounts to putting *two* spikes in the bin which contains  $t$ . Then,

$$\text{Var}(P(\text{spike} | t)) = \langle P^2(\text{spike} | t, \{\mathbf{z}^i\}, M) \rangle - \langle P(\text{spike} | t, \{\mathbf{z}^i\}, M) \rangle^2 \quad (15)$$

## 2.5 Model selection vs. model averaging: how many bins do we need?

To choose the best  $M$  given  $\{\mathbf{z}^i\}$ , or better, a probable range of  $M$ s, we need to determine the model posterior

$$P(M | \{\mathbf{z}^i\}) = \frac{P(\{\mathbf{z}^i\} | M) P(M)}{\sum_m P(\{\mathbf{z}^i\} | m) P(m)} \quad (16)$$

where  $P(M)$  is the prior over  $M$ , which we assume to be uniform. The motivation for this choice is simply that we have no *a priori* preferences for any model complexity, but we would rather drive the choice of  $M$  as completely as possible by the data. The sum in the denominator runs over all values of  $m$  which we choose to include, at most  $m \leq T - 1$ .

Once  $P(M | \{\mathbf{z}^i\})$  is evaluated, we could use it to select the most probable  $M'$ . However, making this decision means 'contriving' information, namely that all of the posterior probability is concentrated at  $M'$ . Thus we should rather average any predictions over all possible  $M$ , even if evaluating such an average has a computational cost of  $O(T^3)$ , since  $M \leq T - 1$ . If the structure of the data allow, it is possible, and useful given a large enough  $T$ , to reduce this cost by finding a range of  $M$ , such that the risk of excluding a model even though it provides a good description of the data is low. In analogy to the significance levels of orthodox statistics, we shall call this risk  $\alpha$ . If the posterior of  $M$  is unimodal (which it has been in most observed cases, see fig.2, C, for

an example), we can then choose the smallest interval of  $M_s$  around the maximum of  $P(M|\{\mathbf{z}^i\})$  such that

$$P(M_{min} \leq M \leq M_{max}|\{\mathbf{z}^i\}) \leq 1 - \alpha \quad (17)$$

and carry out the averages over this range of  $M$  after renormalising the model posterior. We use  $\alpha = 0.1$  unless stated otherwise.

### 3 Simulations and comparison to other methods

#### 3.1 Predicted PSTH convergence to simulated generator

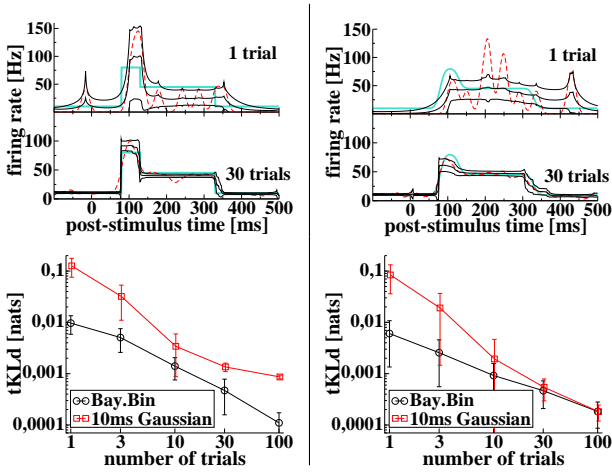


**Fig. 3** Performance comparison on artificially generated spiketrains. The generators (thick, square-wave (left) and smoothed square-wave (right) lines in top panels) are the rate profiles from which the spike trains were drawn. *Top panels* show typical PSTH/SDFs obtained from datasets containing 1 and 30 trials. ‘Typical’ means that the time-averaged Kullback-Leibler divergence (tKLD) between the generator and the estimated PSTH/SDFs is close to the average tKLD for a given number of trials. *Dashed*: smoothing with a Gaussian kernel of 10ms width, *Solid*: Bayesian binning. *Bottom panels*: average tKLD between generator and estimated PSTH/SDFs across 100 simulations as a function of trials per dataset. The generator on the left is comprised of bins, which Bayesian binning should be able to model perfectly given a large enough dataset size. Thus, the tKLD at 100 trials is much smaller for Bayesian binning. More importantly, Bayesian binning is consistently better than Gaussian smoothing even for very small numbers of trials. The generator on the right is smoothed with a 10ms wide Gaussian kernel. While Bayesian binning can no longer model it perfectly with a finite number of bins, it is still a better estimator than kernel smoothing up to at least 100 trials.

We first tested our method by inferring PSTH/SDFs from artificial data. We generated spiketrains from inhomogeneous Bernoulli processes with the rate profiles shown in the top panels of fig.3. To quantify the difference between the generator and an inferred PSTH/SDF, we employed a time-averaged version of the Kullback-Leibler divergence (KLD) (Cover and Thomas

1991). Let  $P(t)$  and  $Q(t)$  be the spiking probability of the generator and the inferred PSTH/SDF at time  $t$ , respectively. The KLD between them at  $t$  is

$$\text{KLD}(t) = P(t) \log \left( \frac{P(t)}{Q(t)} \right) + (1 - P(t)) \log \left( \frac{1 - P(t)}{1 - Q(t)} \right). \quad (18)$$

KLD has several interpretations, the one most relevant for our purposes is the following: if we had observed a spike at time  $t$ ,  $\log \left( \frac{P(t)}{Q(t)} \right) = \log_2(P(t)) - \log_2(Q(t))$  would measure how much more (log-) probable that spike would have been given the generator versus the inferred PSTH/SDF. Likewise, if we had observed no spike,  $\log \left( \frac{1 - P(t)}{1 - Q(t)} \right)$  tells us how much more (log-) probable this event would have been. To get the expected gain in (log-)probability, we need to average these terms over the spike/no spike generating distribution at  $t$ , which is given by  $P(t)$  and  $1 - P(t)$ , respectively. This averaging yields eqn.(18). It can be shown (Cover and Thomas 1991) that  $\text{KLD} \geq 0$  with equality only if  $P(t) = Q(t)$ , i.e. the expected log probability of spike/no spike is maximised by the generating distribution. We average  $\text{KLD}(t)$  across all time indexes of interest to yield the time-averaged KLD (tKLD):

$$\text{tKLD} = \frac{1}{T} \sum_{t=0}^{T-1} \text{KLD}(t) \quad (19)$$

The top panels in fig.3 show typical PSTH/SDFs inferred from 1 and 30 trials. ‘Typical’ means that the tKLD is close to the average tKLD for a given number of trials. The Bayesian binning PSTH is computed from the predictive firing probability  $\langle P(\text{spike}|t) \rangle$ , the dashed lines represent  $\pm 1$  posterior standard deviation (from eqn.(15)), the prior parameters  $\sigma_m$  and  $\gamma_m$  were equal for all bins and set to their maximum a-posteriori value. The generating rate profile in the left half of fig.3 is comprised of bins. Hence, Bayesian binning should model it with increasing accuracy and reduced uncertainty as the dataset grows. An indication for that can be seen by comparing the PSTH/SDFs from 1 and 30 trials: the generating rate profile is followed much more closely for 30 trials than for 1 and the posterior standard deviations also decrease noticeably as the number of trials increases. Furthermore, the Bayesian binning PSTH is closer to the generator than the SDF computed by smoothing the spiketrains with a 10ms wide Gaussian kernel, which is displayed for comparison.

Importantly, Bayesian binning is doing well even if the generator cannot be modelled by a small number of bins: the right half of fig.3 shows simulation results for a generator that was smoothed with a 10ms wide Gaussian kernel. Here, the Gaussian kernel smoothing gives expectably good results (at least for 30 trials), but note that Bayesian binning is doing apparently equally as well. More quantitative performance comparison results are shown in the bottom panels of fig.3. We repeated the simulation 100 times for a given number of trials per dataset, thus obtaining the average tKLD and

its standard deviation. For the bin generator, Bayesian binning outperforms Gaussian kernel smoothing for all dataset sizes. For the smoothed generator, Bayesian binning still outperforms Gaussian kernel smoothing, while the difference between the two methods shrinks as the number of trials per dataset increases. But even for 100 trials, Bayesian binning is as good as Gaussian kernel smoothing. We have thus reason to hope that Bayesian binning might outperform other PSTH/SDF estimation methods on real neural data. This will be shown in the next subsections.

### 3.2 Data acquisition

The experimental protocols have been described before (Oram et al 2002; van Rossum et al 2008). Briefly, extra-cellular single-unit recordings were made using standard techniques from the upper and lower banks of the anterior part of the superior temporal sulcus (STSa) of two monkeys (*Macaca mulatta*) performing a visual fixation task. The subject received a drop of fruit juice reward every 500ms of fixation while static stimuli ( $10^\circ$  by  $12.5^\circ$ ) were displayed. Static images were presented centrally on the monitor. Stimuli consisted of 256 gray scale pictures of familiar and unfamiliar objects, heads, body parts and whole bodies. Visual stimuli were presented in a random sequence for 333ms with a 333ms inter-stimulus interval centrally on a black monitor screen (Sony GDM-20D11, resolution 25.7 pixels/degree, refresh rate 72Hz), 57cm from the subject. Stimulus contrast was determined using foreground regions of the image. The 100% Michelson contrast =  $\frac{L_{max}-L_{min}}{L_{max}+L_{min}}$ , where  $L$  is the luminance, was formed by normalising the foreground pixel values such that they occupied the monitor full luminance range after adjusting the initial greyscale image to have mid (50%) luminance. Other contrast versions (75%, 50%, 25%, 12.5%) were achieved by systematically varying the width of the distribution of the foreground pixel values of the 100% contrast version while maintaining the average foreground luminance. All manipulations were performed after correcting for the measured gamma function of the display monitor.

Stimulus presentation began after 500ms of fixation centrally on the screen (fixation deviations outside the fixation window lasting  $\leq 100$ ms were ignored to allow for blinking). Fixation was rewarded with the delivery of fruit juice. Spikes were recorded during the period of fixation. If the subject looked away for longer than 100ms, both spike recording and presentation of stimuli stopped until the subject resumed fixation for 500ms. The results from initial screening (Edwards et al 2003) were used to select stimuli that elicited large responses from the neuron (effective stimuli) and to select stimuli that elicited small or no response (ineffective stimuli). For different neurons effective and ineffective stimuli included different views of the head (Perrett et al 1991), abstract patterns and familiar objects (Földiák et al

2004). Details of the stimulus selectivity of these neurons has been reported elsewhere (Oram et al 2002; Földiák et al 2004; Edwards et al 2003; Barraclough et al 2005; Edwards et al 2003). The anterior-posterior extent of the recorded cells was from 7mm to 10mm anterior of the interaural plane, in the upper bank (TAa, TPO), lower bank (TEa, TEm) and fundus (PGA, IPa) of the superior temporal sulcus (STS) and in the anterior areas of TE (AIT of [Tanaka1991]), areas which we collectively call the anterior STS (STSa, see (Barraclough et al 2005) for further discussion). The recorded firing patterns were turned into distinct samples, each of which contained the spikes from  $-300$  ms to  $600$  ms after the stimulus onset with a temporal resolution of 1ms.

### 3.3 Inferring PSTHs

To see the method in action on real neural data, inferred a PSTH from 32 spiketrains recorded from one of the available STSa neurons (see fig.1, A). We discretised the interval from  $-100$ ms pre-stimulus to  $600$ ms post-stimulus into  $\Delta t = 1$ ms time intervals and computed the posterior (eqn.(16)) for models with varying number of bins  $M$  (see fig.2, C). The prior parameters were equal for all bins and set to  $\sigma_m = 1$  and  $\gamma_m = 32$ . This choice corresponds to a firing probability of  $\approx 0.03$  in each 1 ms time interval (30 spikes/s), which is typical for the neurons in this study<sup>1</sup>. Models with  $4 \leq M \leq 13$  (expected bin sizes between  $\approx 23$ ms-148ms) were included on an  $\alpha = 0.1$  risk level (eqn.(17)) in the subsequent calculation of the predictive firing rate (i.e. the *expected* firing rate, hence the continuous appearance) and standard deviation (fig.1, D). For comparison, fig.1, B, shows a bar PSTH and a line PSTH computed with the recently developed methods described in (Shimazaki and Shinomoto 2007c,b). Roughly speaking, these methods try to optimise a compromise between minimal within-bin variance and maximal between-bin variance. In this example, the bar PSTH consists of 26 bins. Panel C in fig.1 depicts a SDF obtained by smoothing the spiketrains with a 10ms wide Gaussian kernel, a standard way of calculating SDFs in the neurophysiological literature.

All tested methods produce results which are, upon cursory visual inspection, largely consistent with the spiketrains. However, Bayesian binning is better suited than Gaussian smoothing to model steep changes, such as the transient response starting at  $\approx 100$ ms. While the methods from (Shimazaki and Shinomoto 2007c,b) share this advantage, they suffer from two drawbacks: firstly, the bin boundaries are evenly spaced, hence the peak of the transient is later than visual examination of the rastergrams would suggest. Secondly, because the bin

<sup>1</sup> Alternatively, one could search for the  $\sigma_m, \gamma_m$  which maximise of  $P(\{\mathbf{z}^i\}|\sigma_m, \gamma_m) = \sum_M P(\{\mathbf{z}^i\}|M)P(M|\sigma_m, \gamma_m)$ , where  $P(\{\mathbf{z}^i\}|M)$  is given by eqn.(9). Using a uniform  $P(M|\sigma_m, \gamma_m)$ , we found  $\sigma_m \approx 2.3$  and  $\gamma_m \approx 37$  for the data in fig.1, A

duration is the only parameter of the model, these methods are forced to put many bins even in intervals that are relatively constant, such as the baselines before and after the stimulus-driven response. In contrast, Bayesian binning is able to put bin boundaries anywhere in the time span of interest and can model the data with less bins – the model posterior has its maximum at  $M = 6$  (7 bins), whereas the bar PSTH consists of 26 bins.

### 3.4 Performance comparison by cross-validation

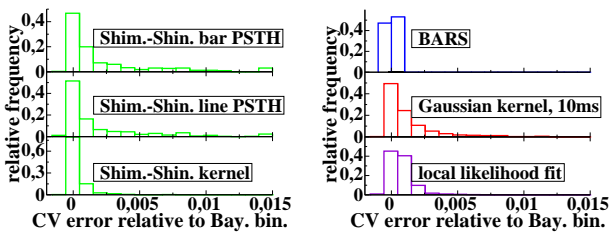


**Fig. 4** Comparison of Bayesian Binning with competing methods by 5-fold crossvalidation. The CV error is the negative expected log-probability of the test data. The histograms show relative frequencies of CV error differences to our Bayesian binning approach. *Left*: Shimazaki’s and Shinomoto’s methods (Shimazaki and Shinomoto 2007b,a). *Right, top*: Bayesian Adaptive Regression Splines (BARS) (DiMatteo et al 2001). *Right, middle*: smoothing with a Gaussian kernel of 10ms width. *Right, bottom*: local likelihood adaptive fitting (Loader 1997, 1999).

For a more rigorous method comparison, we split the data into distinct sets, each of which contained the responses of a cell to a different stimulus. This procedure yielded 336 sets from 20 cells with at least 20 spiketrains per set. We then performed 5-fold crossvalidation. The crossvalidation error is given by the negative logarithm of the predicted probability (eqn.(13)) of the data (spike or no spike) in the test sets. Let  $s_n(t) = 1$  if trial  $n$  of  $N$  in the test set contains a spike at time index  $t \in \{0, \dots, T-1\}$  and  $s_n(t) = 0$  otherwise. Then

$$\text{CV error} = -\frac{1}{N} \sum_{n=0}^{N-1} \frac{1}{T} \sum_{t=0}^{T-1} \log \langle (P(s_n(t)|t)) \rangle. \quad (20)$$

Thus, we measure how well the PSTHs/SDFs predict the test data on average across time and across all test trials. Note that this CV error is similar to the tKLd (eqn.(19)): the constant terms referring to the generator have been dropped, because the generator is not known here and the averaging is done across the data rather than the generating distribution for the same reason. We average the CV error over the 5 estimates to obtain a single estimate for each of the 336 neuron/stimulus combinations. The prior parameters  $\sigma_m, \gamma_m$  were equal for all bins and MAP optimised for each individual training dataset. In (Endres et al 2008) we already

**Table 1** Average log prediction error differences to Bayesian binning from 5 fold crossvalidation on 336 datasets. A positive value means that our method predicts the data better than the competitor.

Method	CV error diff.
Shimazaki and Shinomoto (2007b) bar	$(2.35 \pm 0.23) \times 10^{-3}$
Shimazaki and Shinomoto (2007b) line	$(1.22 \pm 0.10) \times 10^{-3}$
Gauss 10ms	$(1.29 \pm 0.11) \times 10^{-3}$
Local likelihood fit (Loader 1997)	$(7.34 \pm 0.48) \times 10^{-4}$
Shimazaki and Shinomoto (2007a) kernel	$(3.14 \pm 0.39) \times 10^{-4}$
BARS (DiMatteo et al 2001)	$(0.8 \pm 1.6) \times 10^{-5}$
Bayesian binning	0

demonstrated that Bayesian binning outperforms SDFs obtained by Gaussian smoothing, and the bin and line histogram methods from (Shimazaki and Shinomoto 2007c,b).

We also tested Bayesian binning against the kernel smoothing method described in (Shimazaki and Shinomoto 2007a), a local likelihood adaptive fit (Loader 1999) and Bayesian Adaptive Regression Splines (BARS) (DiMatteo et al 2001). To compare the performances between the different methods directly, we calculated the difference in CV error for each neuron/stimulus configuration. Here a positive value indicates that Bayesian binning predicts the test data more accurately than the alternative method. Fig.4, shows the relative frequencies of CV error differences between the other methods and our approach. In the large majority of cases we are at least as good, but frequently better than the competitors, indicating the general utility of our approach. Amongst the competitors, BARS is the only method with a comparable predictive performance on these STS data. The average CV error differences, summarised in table 1, support this claim: they are all significantly  $> 0$ , except for the BARS value.

## 4 Response latency

Besides the instantaneous firing rate, another frequently used feature for the description of a neuron’s response is response latency. But unlike the former, a definition of latency seems much less agreed. A wide range of methods to estimate response latency exist. Changes in phase between neuronal activity and sinusoidal drifting gratings with changing stimulus parameters can provide an indirect measure of response latency (Gawne et al 1996b; Alitto and Usrey 2004). Direct measures of response latency of neurons with low background or spontaneous activity can be obtained from the time of the first spike after stimulus onset (Heil and Irvine 1997; Richmond et al 1999; Syka et al 2000; Stecker and Middlebrooks 2003; Hurley and Pollak 2005; van Rossum et al 2008).

Statistical approaches compare activity levels at two time points. While the baseline level is usually taken from a “pre-stimulus” period the window containing the greatest activ-

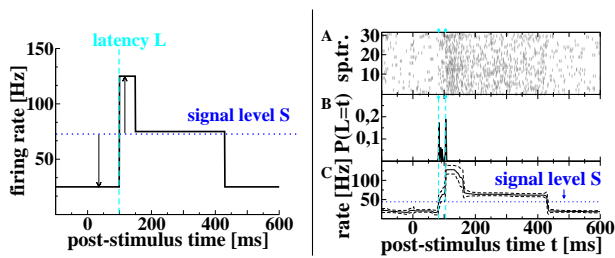


**Fig. 5** *Left*: our minimal latency definition. Latency  $L$  (vertical dashed line) is that point in time before which the firing probability was consistently below the signal level (dotted horizontal line), and after which the firing probability is above the signal level for at least one bin. This definition has two important implications: the latency is at a bin boundary, and there can be at most one latency (possibly none). *Right*: *A*: each tick mark represents a spike, recorded from the same STSa neuron as in fig.1 under high-contrast viewing conditions. *B*: latency posterior. The two modes of  $P(L = t)$  are at 83ms and 104ms after stimulus onset, indicated by the dashed vertical lines. *C*: expected instantaneous firing rates (thick solid line) plus/minus one standard deviation (thin dashed lines). This signal level  $S$  is indicated by the horizontal line. For details, see text.

ity can be used as the reference point (Berenyi et al 2007). Comparison of the baseline or reference activity with the activity in a sliding window using t-tests (Sugase-Miyamoto and 2005; Berenyi et al 2007) can be used to determine the time point at which neuronal activity changes and hence provide an estimate of response latency.

Several approaches use either the PSTH or the SDF to determine neuronal response latency. Latency estimates can be based on peak activity, typically the time at which the mean activity reaches half the amplitude of the peak (baseline +  $0.5 \times (\text{peak} - \text{baseline})$ , e.g. (Gawne et al 1996a; Lee et al 2007)). A statistical method based on a Poisson model compares the mean activity in successive bins during stimulation with a Poisson process estimated from the "pre-stimulus" period (Maunsell and Gibson 1992; Nowak et al 1995; Hanes et al 1995; Thompson et al 1996; Schmolesky et al 2006; Gabel et al 2002; Sary et al 2006). However, Friedman & Priebe (Friedman and Priebe 1998) concluded that a maximum likelihood estimation of parameters for a step change in Poissonian generator (rate 1 pre-latency, rate 2 post-latency) was a better methodology in terms of mean square error than using half-height (Gawne et al 1996a) and the Poisson assumption approach (Maunsell and Gibson 1992).

Some statistical approaches to estimating response latency use measures of the variability obtained from the data rather than assume Poisson statistics. Simple methods estimate response latency as the time point at which activity exceeds baseline plus some error margin (e.g. 1.96 or 2.58 standard error of mean (SEM) of baseline, (Oram and Perrett 1992; Oram and Perret 1996; Tamura and Tanaka 2001; Edwards et al 2003; Eifuku et al 2004; Kiani et al 2005; van Rossum et al 2008). Such thresholding can also determine if a visually induced response is present (e.g. baseline+3.72 SEM, (Lee et al

2007)). Of course, estimates of latency derived from the SDF will vary with the width of the smoothing kernel. Ingenious methods involving estimates from multiple kernels of different widths have been developed to minimise this effect (Liu and Richmond 2000).

Other methods developed to estimate response latency include using ROC analysis of single cell recordings (Tanaka and Lisberger 2002). Estimating response latency as the time of the peak in the derivative of the SDF from multi-unit and local field potential recordings (Fries et al 2001) relies on rapid change in firing rate at response onset. Taking the first time bin of the longest monotonic rise in activity (Liu and Richmond 2000) relies on a large, but not necessarily fast, change in activity. Finally, Luczak and colleagues (Luczak et al 2007) use the mean spike time after stimulus onset as a latency measure.

Methods have also been developed that allow for estimation of the response latency of a single trial. Some calculate the trial-by-trial variability of response latency but do not give the absolute latency (Nawrot et al 2003). Other statistical approaches, including the Poisson based methods (Maunsell and Gibson 1992; Hanes et al 1995; Thompson et al 1996; Sary et al 2006) and the "baseline+error margin" methods, can provide latency estimates for single trials although they may not return a latency estimate for every trial (Friedman and Priebe 1998). The trial alignment approach from (Ventura 2004) builds on the observation that a PSTH, when normalised across time, can be interpreted as a probability distribution for generating spike times. Assuming that the shape of the PSTH does not change across trials, but may be shifted in time relative to other trials, the difference between trial latencies must then be equal to the difference of mean spike times. To compute an absolute latency, (Ventura 2004) recommends to align all trials to the minimal trial mean and use a point estimation method on the aligned trials, since the alignment should facilitate the detection of a sharp onset. Confidence intervals on the latency estimates can be obtained via bootstrap.

We note that most of the methods listed above share the notion of determining latency by estimating a point value. However, with finite data there is always uncertainty in the estimate. For example, when latency is estimated as 100ms it could be 99ms or 101ms with almost as much certainty but is relatively unlikely to be 90 or 110ms. If we want to search for patterns or changes in response latency more exacting analysis techniques should thus incorporate the uncertainty in a principled fashion. We also want a single method that, without any change to parameters or code, works with individual trials, with a set of trials to a single stimulus and with all trials from a neuron. We now develop and evaluate latency estimation using our Bayesian binning technique and show it meets these two criteria.

#### 4.1 A minimal definition of response latency

Most people interested in latency would probably agree with the notion that 'latency is where the signal starts'. Signal vs. no signal can usually be translated into firing rate above or below a threshold, which we will call the *signal level* (see fig.5, left). In other words, *latency is that point in time prior to which there was no signal, and after which there is a signal for at least some duration*. This is the 'minimal' latency definition which we will employ in the following.

For given bin boundaries  $\{k_m\}$  and firing probabilities  $\{f_m\}$ , latency must be at a bin boundary, because firing probabilities are constant within each bin. Note that our latency definition implies that there can be at most one latency. If the firing probabilities are below the signal level in every bin, or if  $f_0$ , the firing rate in the first bin is already above the signal level, then there will be no latency.

To obtain a latency posterior distribution, we formally define the probability that the latency  $L$  is at time index  $t$  given  $\{k_m\}, \{f_m\}, M$  and the signal level  $S \in [0, 1]$  ( $S$  is a firing probability. Division by the discretisation stepsize  $\Delta t$  yields firing rate) as

$$P(L = t | \{k_m\}, \{f_m\}, M, S) = \begin{cases} 1 & \text{if } \exists k_{j-1} \in \{k_m\} : k_{j-1} + 1 = t \\ & \text{and } f_j \geq S \text{ and } \forall m < j : f_m < S \\ 0 & \text{otherwise} \end{cases} \quad (21)$$

which can be exactly averaged over the posterior eqn.(8) by a dynamic programming algorithm similar to that used for the evidence evaluation, as detailed in appendix B. We thus obtain  $P(L = t, \{\mathbf{z}^i\} | M, S)$  and hence, noting that  $P(\{\mathbf{z}^i\} | M) = P(\{\mathbf{z}^i\} | M, S)$ :

$$P(L = t | \{\mathbf{z}^i\}, M, S) = \frac{P(L = t, \{\mathbf{z}^i\} | M, S)}{P(\{\mathbf{z}^i\} | M)}. \quad (22)$$

What remains to be determined is the signal level  $S$ . Assuming that the data span the response range of the neuron (i.e. the data contain responses to at least one effective stimulus), one can proceed as follows: for a given  $S$ , marginalise the latency posterior across the time interval of interest, thereby obtaining the probability  $P(L \text{ exists})$  that a latency exists at that  $S$ . Repeat this procedure for different  $S$  until the maximal  $P(L \text{ exists})$  is found. We use 10 golden section refinement steps (Press et al 1986) for the maximum search with an initial interval of  $[0\text{Hz}, 100\text{Hz}]$ , thereby achieving an accuracy of  $\leq 1\text{Hz}$ .

#### 4.2 Properties of latency posterior distributions

Fig.6 illustrates the consequences of our latency definition on simulated data. We generated 10 spiketrains from inhomogeneous Bernoulli processes with a step in firing rate  $10\text{Hz} \rightarrow 80\text{Hz}$  or  $10\text{Hz} \rightarrow 30\text{Hz}$  at 80ms after stimulus onset.

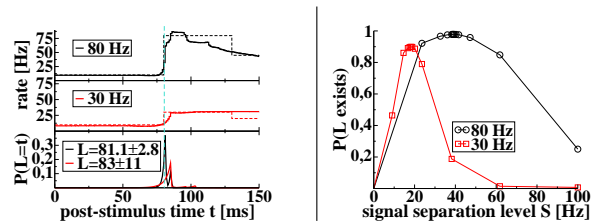


**Fig. 6** Latency posterior and signal separation levels. *Left*: 10 spike-trains were drawn from generators with 80Hz and 30Hz peak firing rate. Both generators had a baseline of 10Hz and a latency at 80ms after stimulus onset. The dashed lines show the generating rates, the solid lines represent the predictive firing rate of the Bayesian binning PSTHs. The resulting latency posterior distributions are shown at the bottom, including the latency expectations  $\pm 1$  posterior standard deviation. The posterior uncertainty in the 30Hz peak rate condition is significantly larger than in the 80Hz condition. *Right*: determination of signal separation level  $S$ .  $P(L \text{ exists})$  is the probability that the latency was somewhere in the latency search interval (here  $[0, 200]$ ms after stimulus onset) given  $S$ . The symbols are located at the points where  $P(L \text{ exists})$  was evaluated by a golden section maximum search (Press et al 1986). The  $S$  was chosen to be the firing rate which maximises the probability that a latency exists. In the 30Hz condition, there is a relatively clear maximum at  $\approx 17\text{Hz}$ , whereas in the 80Hz condition, the maximum is much broader. This is due to the larger difference between baseline and peak firing rate in the latter condition: even for this relatively small dataset (10 trials), there is a range of similarly good signal separation levels that allow for the distinction between baseline and peak firing. For details, see text.

The firing rate stayed at this value for 50ms, then dropped to 45Hz and 20Hz for 200ms before returning to the 10Hz baseline. In both conditions, most of the probability mass of the latency posterior (fig.6, left bottom) is concentrated in the vicinity of the generator's latency. The best signal separation level  $S$  (fig.6, right) for each condition reflects the difference in peak firing rates: for 30Hz,  $S \approx 17\text{Hz}$ , where as for 80 Hz,  $S \approx 39\text{Hz}$ . In both cases,  $S$  is roughly in the middle between baseline and peak firing rate. Latency was searched in the interval  $[0, 200]$ ms after stimulus onset.

In addition to the location of the latency, the latency posterior distributions (fig.6, left bottom) also contain information about uncertainty. It is evident that a smaller step in firing rate leads to a wider latency posterior, which can also be captured by computing the standard deviation from that posterior. This observation is not particularly surprising, but nevertheless important: virtually all other latency estimation methods ignore uncertainty due to their point estimation nature. As a consequence, the latency posterior contains information about the change in firing rate, which is a point that we will return to later (section 5) when we analyse latency and firing rate with information-theoretic methods. Note also that the latency posteriors are far from Gaussian: a description in terms of mean and standard deviation is therefore inadequate for an information-theoretic analysis and might distort conclusions drawn from it.

Non-Gaussian latency posteriors are also observed in the real data. Fig.5, right, has two distinct peaks, the lower one at  $\approx 83$  ms, the higher one being at  $\approx 104$  ms after stimulus onset. The location of these peaks can be understood from the height of the PSTH (fig.5, right, C) relative to the signal level: at 83 ms, one can be fairly certain that the PSTH was below the signal level prior to this time index, and there is a nonzero probability (albeit not nearly certainty) that the PSTH is above the signal level directly afterwards. At 104 ms, the PSTH is above the signal level with near certainty directly after the peak in the latency posterior, whereas one can not be quite sure that the PSTH was below the signal level the interval immediately before this point in time. The expected latency  $\pm$  SEM is  $(94 \pm 10)$ ms. A conventional interpretation of these values would suggest that the bulk of the probability mass can be found close to the mean, which is not true.

### 4.3 Simulation results

For a quantitative evaluation of the accuracy of our latency detection method, we generated spiketrains from inhomogeneous Bernoulli processes with the rate profiles shown in the insets of fig.7. Root-mean-square (RMS) errors were computed from 100 repetitions of the simulation for a given number of trials per dataset, see fig.7. We used the expected latency as the prediction of Bayesian binning for each dataset (similar results were found using a MAP estimate). To further illustrate the performance of our approach, we compared it to three other ways of latency detection: the half-height method (Gawne et al 1996a) ('HH' in fig.7), latency = the first time where activity exceeds baseline rate plus 2 SEM of baseline rate (Oram and Perrett 1992) ('2SD' in fig.7) and the trial alignment approach from (Ventura 2004). This approach yields a relative latency for each trial, absolute latency can be determined by a suitable change-point method applied to the aligned trials. We used the half-height method here, since it gives good estimates of the latency without alignment.

Our method is more accurate than the others in all tested conditions. This is true even if the generator has a sloping response onset (fig.7, right) and can no longer be easily modelled by bins. In this case, latency is not as clearly defined as for a step response onset. We took the point of the first rate inflection at 80ms to be the 'true' latency. Note that this is an additional condition which is not a part of our latency definition. If we had certain knowledge of the generating firing rates, any  $S \in (10\text{Hz}, 80\text{Hz})$  would be suitable as a separation level. A consequence of choosing the first point of inflection as 'true' latency is an increase in RMS of Bayesian binning between 10 and 30 trials for the 80Hz peak, sloping onset condition. This is due to a very flat signal separation maximum (see also fig.6, right), i.e. there are many values

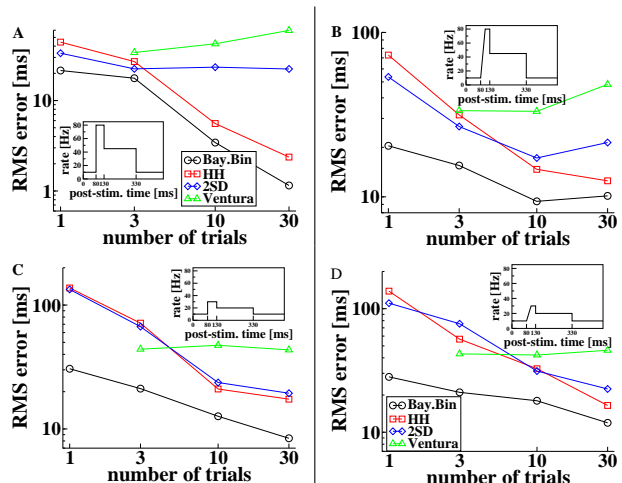


**Fig. 7** Comparison of latency estimates. RMS errors were computed from 100 repetitions of the simulation for a given number of trials per dataset. 'HH' are the results from the half-height method (Gawne et al 1996a), '2SD' determines latency to be the first time where activity exceeds baseline rate plus 2 SEM of baseline rate (Oram and Perrett 1992), 'Ventura' is the trial alignment method from (Ventura 2004) and 'Bay.Bin' shows the RMS errors using the expected latency from our method. Insets show generating rate profiles. *Left*: generators comprised of bins with latency at 80ms. Bayesian binning latency detection outperforms the other methods for all dataset sizes. The high, flat error curve of the 2SD method in the 80Hz peak firing rate condition is due to a consistent underestimation of latency, which is an artifact of Gaussian kernel smoothing combined with a baseline SEM that is small in comparison with the firing rate step at the latency. *Right*: generator with sloping response onsets. We measured the RMS against an assumed latency of 80ms, even though latency is no longer well defined in these conditions. Our Bayesian binning method is still better than the competitors, despite the fact that a slope is hard to model with bins. Its increase in RMS between 10 trials and 30 trials in the high peak firing condition is due to a flat signal separation maximum (see also fig.6, right).

of  $S$  which allow for an almost equally certain separation between 'firing rate above  $S$ ' and 'firing rate below  $S$ '. Since we search for a single maximum, this maximum's location will then mostly be determined by noise, and not by differences in signal quality. If we wanted to bring the  $L$  closer to the first rate inflection point, we would have to optimise a compromise between large  $P(L \text{ exists})$  and small  $S$ . This could be accomplished by adding a weak prior over  $S$  which prefers small  $S$ . However, this is no longer a 'minimal' definition of latency, so we will continue to use our original definition.

### 4.4 Trial-by-trial latency and firing rate estimation

So far, we computed the model posteriors and all quantities derived thereof on the assumption that there is a single 'correct' PSTH from which the data were generated. In other words, we presupposed that the experimentally controlled parameters (e.g. stimulus identity and presentation

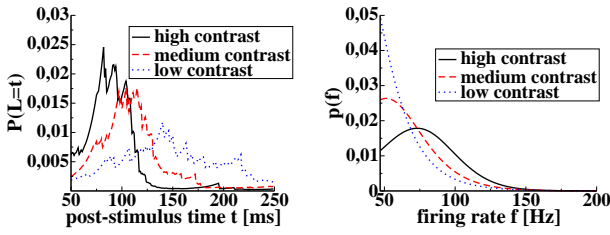


**Fig. 8** Trial-by-trial latency and firing rate posteriors for three stimulus contrasts. *Left*: a latency posterior was computed for each trial and then marginalised across all trials for a given contrast. The high contrast posterior was calculated on the same data as the latency posterior in fig.5, right. While the posterior uncertainty is increased due to the trial-by-trial evaluation, the bulk of the probability is in the same post-stimulus time range ( $\approx 75\text{ms}$ - $110\text{ms}$ ) as before. Reducing stimulus contrast clearly increases latencies. *Right*: firing rate posterior densities in the first bin after the latency.

time) were enough to specify the spike train generating process up to a random element, which is fully modelled by the firing probability. One might object to this model. It is certainly conceivable that for instance latencies and firing rates of the generator vary between trials. Therefore, it would be desirable to be able to compute the posterior distributions of these parameters on a trial-by-trial basis. It is possible to do that with our method, as indicated by the single trials performances in simulations (see fig.3 and fig.7). Fig.8, left, shows a trial-by-trial latency posterior distribution marginalised across all trials to stimuli of high (100%), medium (50%) and low (12.5%) contrast. The high contrast latency posterior was calculated on the same data as those used in fig.5, right. While the posterior uncertainty is increased due to the trial-by-trial evaluation, the bulk of the probability is in the same post-stimulus time range ( $\approx 75\text{ms}$ - $110\text{ms}$ , with  $S \approx 47\text{Hz}$ ) as before. Moreover, it is apparent that latency increases with decreasing stimulus contrast, which was also observed in (Oram et al 2002) using a statistical approach (Oram and Perrett 1992; Oram and Perrett 1996).

To calculate the posterior distribution of firing rates across trials, one can proceed in a fashion similar to that used for latency: define the probability density that the firing rate at  $t$ ,  $f(t)$ , is  $\tilde{f}$  given the model parameters as

$$p(f(t) = \tilde{f} | \{k_m\}, \{f_m\}, M) = \begin{cases} \delta(f_j - \tilde{f}) & \text{if } t \in \{k_{j-1} + 1, \dots, k_j\} \\ 0 & \text{otherwise} \end{cases} \quad (23)$$

where  $\delta(x)$  is the Dirac delta function. In words, this probability density is concentrated at the firing rate  $f_j$  of that bin which contains the time index  $t$  if  $f_j = \tilde{f}$ . By adding the condition that the lower bound of bin  $j$  is equal to the latency, we can compute the probability density of the firing rate in the first bin after the latency, i.e. in the strong transient part of the response. If  $\{k_m\}$  and  $\{f_m\}$  are given, then this firing

rate  $f_j$  depends on the latency only through the signal level  $S$ , because  $f_j \geq S$  (see eqn.(21)). Thus, we can compute the joint probability (density) of 'latency  $L = t$ ' and 'firing rate is  $\tilde{f}$ ' by multiplying the r.h.s of eqn.(23) with the r.h.s of eqn.(21) if  $\tilde{f} \geq S$ :

$$p(f(t) = \tilde{f}, L = t | \{k_m\}, \{f_m\}, M, S) = \begin{cases} p(f(t) = \tilde{f} | \{k_m\}, \{f_m\}, M) \times \\ \quad \times P(L = t | \{k_m\}, \{f_m\}, M, S) & \text{if } \tilde{f} \geq S \\ 0 & \text{otherwise.} \end{cases} \quad (24)$$

Averaging this probability density over the posterior eqn.(8) is done by an algorithm similar to the one used for latency, as detailed in appendix C. This yields  $P(f(t) = \tilde{f}, L = t, \{\mathbf{z}^i\} | M, S)$ . Therefore we have

$$p(f(t) = \tilde{f} | L = t, \{\mathbf{z}^i\}, M, S) = \frac{p(f(t) = \tilde{f}, L = t, \{\mathbf{z}^i\} | M, S)}{P(L = t, \{\mathbf{z}^i\} | M, S)} \quad (25)$$

i.e. the probability density of the firing rate being  $\tilde{f}$  given that the latency is at  $t$ , the signal level is  $S$  and the data  $\{\mathbf{z}^i\}$  for a model with  $M$  bins. Averaging this firing rate density across trials yields fig.8, right. Here, firing rates were found to decrease with stimulus contrast. Furthermore, the posteriors are unimodal – this indicates that modelling the trial-by-trial variations in firing rate by e.g. a mixture of binomial with a unimodal mixing distribution might be a viable strategy.

## 5 Information-theoretic analysis of latency and firing rate

It is often interesting to quantify the amount of information which a neural response carries about various stimulus parameters. Information theory (Shannon 1948) provides the mathematical framework to address this question: *mutual information*  $I(U; C)$  (Cover and Thomas 1991) measures how much we can expect to learn about a (discrete) stimulus parameter  $C$  from a (discrete) neural response measure  $U$ , and vice versa. Given a joint probability distribution  $P(U, C)$ ,  $I(U; C)$  is defined as

$$I(U; C) = \sum_C \sum_U P(U, C) \log \left( \frac{P(U, C)}{P(U)P(C)} \right) \quad (26)$$

where  $P(U) = \sum_C P(U, C)$  and likewise for  $P(C)$ . If a second neural response measure  $V$  and the joint probability distribution  $P(U, V, C)$  is available, it is possible to define *conditional mutual information*  $I(U; C | V)$  and *joint mutual information*  $I(U, V; C)$  (Cover and Thomas 1991):

$$I(U; C | V) = \sum_C \sum_U \sum_V P(U, V, C) \log \left( \frac{P(U, C | V)}{P(U | V)P(C | V)} \right) \quad (27)$$

$$I(U, V; C) = \sum_C \sum_U \sum_V P(U, V, C) \log \left( \frac{P(U, V, C)}{P(U, V)P(C)} \right) = I(U; C | V) + I(V; C) \quad (28)$$

$I(U;C|V)$  can be understood as the amount of information we expect to gain about  $C$  by observing  $U$  if we knew  $V$ , whereas  $I(U,V;C)$  is the expected information gain about  $C$  if we learned the values of both  $U$  and  $V$ . Extending these definitions to continuous variables is straightforward (Cover and Thomas 1991).

In sections 4.1 and 4.4, we developed the formalism to compute the posterior distribution of the latency  $L$  (eqn.(22)) and the posterior density of the firing rate  $f(t)$  in the first bin after latency (eqn.(25)), providing the joint density

$$p(f(t) = \tilde{f}, L = t | \{\mathbf{z}^i\}, M, S) = p(f(t) = \tilde{f} | L = t, \{\mathbf{z}^i\}, M, S) P(L = t | \{\mathbf{z}^i\}, M, S) \quad (29)$$

which we need to compute joint, conditional and marginal mutual informations between  $L$ ,  $f(t)$  and any stimulus parameter. Note that these distributions/densities are conditioned on the signal level  $S$ . So far, we described a procedure to determine  $S$  for a single stimulus condition  $C$  (see end of section 4.1). We define  $S$  for multi-valued  $C$  based on two assumptions:

1. the signal level  $S$  is a property of the cell, not of the stimulus. In other words, there is a single  $S$  per cell across all  $C$ . If  $S$  was allowed to vary with  $C$ , the choice of  $S$  would inject stimulus-related information into the information estimates which is not present in the data.
2.  $S$  is determined by maximising the marginal probability of latency existence  $P(L \text{ exists} | S)$  (and therefore, signal existence)

$$P(L \text{ exists} | S) = \sum_C P(L \text{ exists} | S, C) P(C) \quad (30)$$

where  $P(C)$  is the prior probability of each stimulus condition, which is controlled by the experimenter.

3. We assume that there is no *a-priori* dependency between  $S$  and  $C$ .

Assumption 2 is a consequence of the experimental design which we are about to analyse. Cells and stimuli were selected such that there was at least one stimulus which evoked a strong response, and at least one that evoked a weak response (possibly none). Maximising the marginal probability of latency existence thus has the effect of choosing an  $S$  such that as many stimulus conditions as possible have a detectable latency. If there is a strong and a weak (but still detectable) response, this procedure chooses a relatively small  $S$  such that  $P(L \text{ exists} | S, C)$  is high for both  $C$ . However, if there is a strong and a non-detectable response, the value of  $S$  will be higher, since it will be driven only by the strong response. It remains to be seen if this procedure needs to be adapted for different cell/stimulus choices.

## 5.1 Results on simulated data

We mentioned in section 4.2 that the latency posterior inevitably contains information about the change in firing rate

at the latency. To illustrate this point, we performed an information-theoretic analysis of a two-stimulus scenario on simulated data. Each stimulus evoked a 50ms long transient response, followed by a sustained response (duration 250ms) with a firing rate between the transient and the 10Hz baseline. In the 'no difference' condition, the two simulated responses had the same underlying generator. We also varied just the firing rate (transient: 100Hz vs. 30Hz), just the latency (80ms vs. 90ms) or both firing rate and latency. Each dataset contained 10 trials per stimulus and was analysed trial-by-trial (i.e. one PSTH inferred per trial). The average results from 10 repetitions of the simulations are summarised in table 2. This table shows the mutual informations between stimulus identity  $C$ , and the variables:

- $E$ : latency exists, i.e.  $L \in \{30ms, \dots, 250ms\}$ .
- $L$ :  $L = t$  for  $t \in \{30ms, \dots, 250ms\}$ , see eqn.(22). Additionally,  $L$  has a special value indicating that a latency does not exist (i.e. no transition from below the signal threshold  $S$  to above  $S$ ).
- $f$ : firing probability  $f(t) = \tilde{f}$  in the first bin after latency for  $\tilde{f} \in [S, 1]$ , see eqn.(25).  $f$  also has a special value indicating that a firing probability in the first bin after latency does not exist.

Note that both  $L$  and  $f$  determine  $E$ : if latency is somewhere in the latency search interval or if the firing rate in the first bin after latency is somewhere above the signal level, then  $E$  is true, otherwise  $E$  is false.  $E$  can also be read as 'firing rate went above the signal level  $S$  somewhere in the latency search interval', and might therefore be viewed as a firing rate related variable, rather than a property of latency. This ambiguity highlights the difficulty of separating firing rate and latency related information, which is due to latency being defined by a firing rate based criterion. We choose to interpret  $E$  as carrying firing rate information, since latency is concerned with the *timing* of response onset, rather than just the presence or absence of a response. Thus, information about  $C$  in  $L$  is given by the conditional mutual information  $I(L;C|E)$ .

The values in the 'no difference' condition in table 2 represent the overestimation biases of our method in this scenario. Overestimation of mutual information (and the closely related underestimation of entropy) from small datasets is a well-known problem, and many remedies have been devised for it (Optican et al 1991; Panzeri and Treves 1996; Nemenman et al 2004; Paninski 2004; Endres and Földiák 2005). However, most of these methods assume a set of datapoints as a starting point, not a set of posterior distributions. Hence, they can not be applied to our analysis unaltered. Further work will be needed to understand how best to provide, within our analysis framework, information estimates whose overestimation is as small as possible.

If there is only a difference in firing rates, then  $I(f;C) > I(L;C|E)$  but  $I(L;C|E)$  is still significantly greater than in

**Table 2** Mutual information  $I$  in [bit] for simulated neurons with a baseline firing rate of 10Hz, trial-by-trial analysis.  $C$  is stimulus identity, there were two stimuli.  $L$  is latency,  $f$  is firing rate in the first bin after latency and latency existence is  $E$ . The latter is the truth value of the proposition 'Latency is somewhere between 30ms and 250ms after stimulus onset'. Difference in  $f$  means that the peak firing rates were 30Hz for one stimulus and 100Hz for the other, duration of peak response 50ms, latency 80ms after stimulus onset. In the 'difference in  $L$ ' condition, both neurons had a peak firing rate of 100Hz for 50ms, with a latency of 80ms for one stimulus and 90ms for the other. 'No difference' means that both peak firing rates (100Hz) and latencies (80ms) were equal. Errors are SEM computed from 10 repetitions of the simulations. For details, see text.

Difference in	$I(E;C)$	$I(L;C E)$	$I(f;C)$
no difference	$0.002 \pm 0.001$	$0.045 \pm 0.004$	$0.008 \pm 0.002$
$f$ : 100/30Hz	$0.255 \pm 0.023$	$0.079 \pm 0.014$	$0.314 \pm 0.023$
$L$ : 80/90ms	$0.007 \pm 0.002$	$0.084 \pm 0.010$	$0.016 \pm 0.004$
$f$ : 100/30Hz, $L$ : 80/90ms	$0.206 \pm 0.026$	$0.072 \pm 0.007$	$0.265 \pm 0.023$

the 'No difference' condition. In other words, even though the simulated cells were designed to have the same latency (80ms), the latency posterior distributions inferred from a finite sample carry information about the magnitude of the firing rate change – a large response allows for the determination of latency with greater certainty than a small one. Compare this to the 'difference in  $L$ ' condition: while  $I(L;C|E)$  is about as large as before,  $I(L;C|E) > I(f;C)$ , i.e. our method is able to distinguish between (un)certainly related and variability related latency information via the information in  $f$ . Furthermore, in both 'difference in  $f$ ' conditions,  $E$  contains a large fraction of the firing rate information, i.e. knowing whether the signal threshold was crossed is the most informative aspect of  $f$ .

In summary, our method yields the results one would expect for each condition: if the stimulus identity  $C$  is encoded in  $f$ , then  $I(f;C)$  is maximal, if changes in  $C$  cause changes in  $L$ ,  $I(L;C|E)$  is maximal. If both  $L$  and  $f$  are influenced by  $C$ , then both can be used together to determine  $C$ .

## 5.2 Results on STSa data

It is known that stimulus contrast influences latency of STSa neurons (Oram et al 2002; van Rossum et al 2008). We now examine responses to high-contrast presentations to ask whether latency changes convey stimulus identity related information in the absence of contrast change. The results of a trial-by-trial analysis of mutual informations computed from 29 STSa neurons under high-contrast viewing conditions are shown in table 3. Entropy of stimulus identity  $C$  is  $H(C) \approx 1$  bit for all cells. Since  $I(f;C) > I(L;C|E)$ , firing rate  $f$  in the first bin after latency carries slightly more information about  $C$  than latency  $L$ , but the difference is not significant. The joint code of latency and firing rate is almost as informative

**Table 3** Average trial-by-trial mutual informations and standard errors of the mean (SEM) computed from 29 STSa neurons under high-contrast viewing conditions. Entropy of stimulus identity  $C$  is  $H(C) \approx 1$  bit for all cells.  $E$ ,  $L$  and  $f$  have the same meaning as in table 2. Firing rate  $f$  in the first bin after latency carries slightly more information about stimulus identity  $C$  than latency  $L$ . For details, see text.

Mutual information between $C$ and		average $\pm$ SEM [bit]
signal existence $E$	$I(E;C)$	$0.0594 \pm 0.0191$
latency $L$ given $E$	$I(L;C E)$	$0.0650 \pm 0.0075$
firing rate $f$	$I(f;C)$	$0.0730 \pm 0.0205$
firing rate given latency	$I(f;C L)$	$0.0136 \pm 0.0020$
latency given firing rate	$I(L;C f)$	$0.0649 \pm 0.0077$
joint code	$I(f,L;C)$	$0.1379 \pm 0.0074$

as the sum of the individual codes,  $I(f,L;C) \approx I(f;C) + I(L;C|E)$ . This is also indicated by  $I(L;C|f) \approx I(L;C|E)$ : the stimulus identity information in firing rate which is redundant with latency is almost completely contained in  $E$ . In other words, the most informative firing rate feature is whether the firing rate crosses the signal threshold or not. To decode stimulus identity, we should therefore answer questions about latency and firing rate in the following order of importance: *has* the cell fired above  $S$ , *when* has it fired above  $S$ , *how much* has it fired above  $S$ ? While these conclusions are certainly conditioned on our small stimulus set (2 stimuli per cell), the values of the mutual informations are small compared to the theoretical maximum of 1 bit. This makes ceiling effects unlikely.

## 6 Summary

We have extended our exact Bayesian binning method (Endres et al 2008) for the estimation of PSTHs. Besides treating uncertainty – a real problem with small neurophysiological datasets – in a principled fashion, it also outperforms several competing methods on real neural data. Amongst the competitors, we found that only BARS (DiMatteo et al 2001) offers comparable predictive performance. However, BARS requires sampling to compute posterior averages, which can potentially take very long or even get stuck, a problem which we observed on data sets containing only a small number of spikes. Bayesian binning allows for the exact evaluation of posterior averages (within numerical roundoff errors) independent of the contents of the data set. It also offers automatic complexity control because the model posterior can be evaluated. While its computational cost is significant, it is still fast enough to be useful: evaluating the predictive probability takes less than 1s on a modern PC<sup>2</sup>, with a small memory footprint (<10MB for 512 spiketrains). We showed how our approach can be adapted to extract characteristic features of neural responses in a Bayesian way, e.g. response

<sup>2</sup> 3.2 GHz Intel Xeon™, SuSE Linux 10.1

latencies or firing rate distributions. But we are not restricted these features: we can use our method to compute expectations of any function of the PSTH, subject to the condition that the function depends on the PSTH in a bin-wise fashion. A free software implementation is available at the machine learning open source software repository<sup>3</sup>. This implementation contains a short tutorial, computes expected PSTH and posterior standard deviations, separation level and latency posterior. It also allows for the optimisation of the prior hyperparameters. The code for the information theoretic calculations is available from the authors on request, but it requires a cluster computer to run efficiently: the integration over the posterior distribution of the firing rate needs to be done numerically and is time consuming ( $\approx$  1-2 days per processor per spiketrain for a trial-by-trial analysis).

The latency alignment procedure of Ventura (2004) was developed to quantify trial-by-trial variation of the response latencies, and as such was not intended to determine an absolute latency estimate. However, Ventura (2004) suggested that the minimal latency estimate from the individual trials could be used. We find this yields a poor estimate of absolute latency which tends to get worse with increasing number of trials. We therefore used the half height method from (Gawne et al 1996a) on the aligned spiketrains to improve the absolute latency estimate. This appears to make the estimate largely independent of the number of trials (see fig.7). In the majority of cases, this procedure still underestimates the absolute latency, since the trials are aligned to the minimal trial latency. To counter this systematic underestimation, we experimented with shifting all aligned trials by the difference between the total pre-alignment and post-alignment means, thereby restoring the original total mean spike time. However, this did not improve results notably. Aligning trials by mean spike time works well on relatively regular spiketrains (such as the gamma order 8 ISI distribution simulations used in (Ventura 2004)). In our simulations with short transients and Bernoulli spike generation, it appears not to work. We would therefore conclude that the poor performance of this method is due to poor estimates of the mean spike time of each trial.

Substituting our observation model eqn.(2) with any other distribution is straightforward, as long as the replacement is also comprised of bins. One might e.g. model each spike train within a bin by a separate Bernoulli process and mix these with a suitable distribution to capture the inter-trial differences. Alternatively, one could use a model similar to that of (Shinomoto and Koyama 2007): choose a Gamma process for the inter-spike intervals and model the time-dependent rate with a bin model.

There are a number of other approaches to PSTH/SDF estimation which were not included in our comparisons. Perhaps most noteworthy (from a Bayesian perspective) are (Shinomoto and Koyama

2007) and a recent Gaussian process model (Cunningham et al 2008). We have not yet directly compared our method to either of them. Comparisons to (Cunningham et al 2008) and (Shinomoto and Koyama 2007) will be interesting future work, once the authors of these works release their code.

Finally, we used our approach to compute exact (up to roundoff errors) expectations of information-theoretic quantities, e.g. mutual informations between latency, firing rate and stimulus identity. We demonstrated that STS neurons convey most of the information about stimulus identity through changes in firing rate. Specifically, we found that the crossing of a signal threshold  $S$  is the most informative firing rate feature. However, extra information about stimulus identity can be gained by looking at the response latency.

**Acknowledgements** D. Endres was supported by a Medical Research Council (UK) special training fellowship in bioinformatics G0501319. Both authors would like to thank P. Földiák and J. Schindelin for stimulating discussions and comments on the manuscript. Data collection was supported by EU framework grant (FP5-Mirror) to M. Oram. We thank the unknown reviewers for their clarifying suggestions and references.

## Appendix A: Computing the evidence with dynamic programming

The evidence, or marginal likelihood of a model with  $M$  bins is given by (see eqn.(9)):

$$P(\{\mathbf{z}^i\}|M) = \sum_{k_{M-1}=M-1}^{T-2} \sum_{k_{M-2}=M-2}^{k_{M-1}-1} \dots \sum_{k_0=0}^{k_1-1} P(\{\mathbf{z}^i\}|\{k_m\}, M) P(\{k_m\}|M) \quad (\text{A-1})$$

where the summation boundaries are chosen such that the bins are non-overlapping and contiguous and

$$P(\{\mathbf{z}^i\}|\{k_m\}, M) = \int_0^1 d\{f_m\} P(\{\mathbf{z}^i\}|\{f_m\}, \{k_m\}, M) p(\{f_m\}|M). \quad (\text{A-2})$$

Recall that the probability of a (multi)set of spiketrains  $\{\mathbf{z}^i\} = \{z_1, \dots, z_N\}$ , assuming independent generation, is given by eqn.(3):

$$P(\{\mathbf{z}^i\}|\{f_m\}, \{k_m\}, M) = \prod_{i=1}^N \prod_{m=0}^M f_m^{s(\mathbf{z}^i, m)} (1 - f_m)^{g(\mathbf{z}^i, m)} = \prod_{m=0}^M f_m^{s(\{\mathbf{z}^i\}, m)} (1 - f_m)^{g(\{\mathbf{z}^i\}, m)} \quad (\text{A-3})$$

where  $s(\{\mathbf{z}^i\}, m) = \sum_{i=1}^N s(\mathbf{z}^i, m)$  is the number of spikes in all spike-trains in bin  $m$  and  $g(\{\mathbf{z}^i\}, m) = \sum_{i=1}^N g(\mathbf{z}^i, m)$  is the number of all non-spikes, or gaps. The prior of the firing rates (eqn.(5)) is

$$p(\{f_m\}|M) = \prod_{m=0}^M \mathbf{B}(f_m; \sigma_m, \gamma_m). \quad (\text{A-4})$$

The integrals in eqn.(A-2) can be evaluated by virtue of eqn.(A-3) and eqn.(A-4):

$$P(\{\mathbf{z}^i\}|\{k_m\}, M) = \prod_{m=0}^M \frac{\mathbf{B}(s(\{\mathbf{z}^i\}, m) + \sigma_m, g(\{\mathbf{z}^i\}, m) + \gamma_m)}{\mathbf{B}(\sigma_m, \gamma_m)} \quad (\text{A-5})$$

<sup>3</sup> <http://www.mloss.org, package 'binsdfc'>.

where  $B(x, y) = \frac{\Gamma(x)\Gamma(y)}{\Gamma(x+y)}$  is Euler's Beta function (Davis 1972). Eqn.(A-5) is a product with one factor per bin, and each factor depends only on spike/gap counts and prior parameters in that bin. To compute eqn.(A-1), we can therefore use an approach very similar to that described in (Endres and Földiák 2005; Endres 2006) in the context of density estimation and in (Hutter 2006, 2007) for Bayesian function approximation: define the function

$$\text{getIEC}(k_s, k_e, m) := B(s(\{\mathbf{z}^i\}, k_s, k_e) + \sigma_m, g(\{\mathbf{z}^i\}, k_s, k_e) + \gamma_m) \quad (\text{A-6})$$

where  $s(\{\mathbf{z}^i\}, k_s, k_e)$  is the number of spikes and  $g(\{\mathbf{z}^i\}, k_s, k_e)$  is the number of gaps in  $\{\mathbf{z}^i\}$  between the start interval  $k_s$  and the end interval  $k_e$  (both included). Furthermore, collect all contributions to eqn.(A-1) that do not depend on the data (i.e.  $\{\mathbf{z}^i\}$ ) and store them in the array  $\text{pr}[M]$ :

$$\text{pr}[M] := \frac{\prod_{m=0}^M \frac{1}{B(\sigma_m, \gamma_m)}}{\binom{T-1}{M}}. \quad (\text{A-7})$$

Substituting eqn.(A-5) into eqn.(A-1) and using the definitions (A-6) and (A-7), we obtain

$$P(\{\mathbf{z}^i\}|M) \propto \sum_{k_{M-1}=M-1}^{T-2} \dots \sum_{k_0=0}^{k_1-1} \prod_{m=1}^M \text{getIEC}(k_{m-1} + 1, k_m, m) \times \text{getIEC}(0, k_0, 0) \quad (\text{A-8})$$

with  $k_M = T - 1$  and the constant of proportionality being  $\text{pr}[M]$ . Since the factors on the r.h.s. depend only on two consecutive bin boundaries each, it is possible to apply dynamic programming (Bertsekas 2000): rewrite the r.h.s. by 'pushing' the sums as far to the right as possible:

$$P(\{\mathbf{z}^i\}|M) \propto \sum_{k_{M-1}=M-1}^{T-2} \text{getIEC}(k_{M-1} + 1, T - 1, M) \times \sum_{k_{M-2}=M-2}^{k_{M-1}-1} \text{getIEC}(k_{M-2} + 1, k_{M-1}, M - 1) \times \dots \sum_{k_0=0}^{k_1-1} \text{getIEC}(k_0 + 1, k_1, 1) \text{getIEC}(0, k_0, 0). \quad (\text{A-9})$$

Evaluating the sum over  $k_0$  requires  $O(T)$  operations (assuming that  $T \gg M$ , which is likely to be the case in real-world applications). As the summands depend also on  $k_1$ , we need to repeat this evaluation  $O(T)$  times, i.e. summing out  $k_0$  for all possible values of  $k_1$  requires  $O(T^2)$  operations. This procedure is then repeated for the remaining  $M - 1$  sums, yielding a total computational effort of  $O(MT^2)$ . Thus, initialise the array  $\text{subE}_0[k] := \text{getIEC}(0, k, 0)$ , and iterate for all  $m = 1, \dots, M$ :

$$\text{subE}_m[k] := \sum_{r=m-1}^{k-1} \text{getIEC}(r + 1, k, m) \text{subE}_{m-1}[r], \quad (\text{A-10})$$

A close look at eqn.(A-9) reveals that while we sum over  $k_{M-1}$ , we need  $\text{subE}_{M-1}[k]$  for  $k = M - 1; \dots; T - 2$  to compute the evidence of a model with its latest boundary at  $T - 1$ . We can, however, compute  $\text{subE}_{M-1}[T - 1]$  with little extra effort, which is, up to a factor  $\text{pr}[M - 1]$ , equal to  $P(\{\mathbf{z}^i\}|M - 1)$ , i.e. the evidence for a model with  $M - 1$  bin boundaries. Moreover, having computed  $\text{subE}_m[k]$ , we do not need  $\text{subE}_{m-1}[k - 1]$  anymore. Hence, the array  $\text{subE}_{m-1}[k]$  can be reused to store  $\text{subE}_m[k]$ , if overwritten in reverse order. Table A-T1 shows this algorithm in pseudo-code (E[m] contains the evidence of a model with  $m$  bin boundaries inside  $[t_{\min}, t_{\max}]$  after termination).

**Table A-T1** Computing the evidences of models with up to  $M$  bin boundaries

1. for  $k := 0 \dots T - 1$ :  $\text{subE}[k] := \text{getIEC}(0, k, 0)$
2.  $E[0] := \text{subE}[T - 1] \times \text{pr}[0]$
3. for  $m := 1 \dots M$ :
  - (a) if  $m = M$  then  $l := T - 1$  else  $l := m$
  - (b) for  $k := T - 1 \dots l$ 

$$\text{subE}[k] := \sum_{r=m-1}^{k-1} \text{subE}[r] \times \text{getIEC}(r + 1, k, m)$$
  - (c)  $E[m] = \text{subE}[T - 1] \times \text{pr}[m]$
4. return E[]

## Appendix B: Computing the posterior distribution of the latency

We compute the joint probability of the latency  $L = t$  and the observed spiketrains  $\{\mathbf{z}^i\}$  given the number of bins and the signal separation level  $S$  via

$$P(L = t, \{\mathbf{z}^i\}|M, S) = \sum_{k_{M-1}=M-1}^{T-2} \sum_{k_{M-2}=M-2}^{k_{M-1}-1} \dots \sum_{k_0=0}^{k_1-1} P(L = t, \{\mathbf{z}^i\}, \{k_m\}|M, S) \quad (\text{B-11})$$

where

$$P(L = t, \{\mathbf{z}^i\}, \{k_m\}|M, S) = \int_0^1 d\{f_m\} P(L = t | \{k_m\}, \{f_m\}, M, S) p(\{\mathbf{z}^i\}, \{f_m\}, \{k_m\}|M). \quad (\text{B-12})$$

Note that  $P(L = t | \{k_m\}, \{f_m\}, M, S)$  is the r.h.s. of eqn.(21) and  $p(\{\mathbf{z}^i\}, \{f_m\}, \{k_m\}|M)$  is the numerator of the r.h.s. of eqn.(8). As a consequence of eqn.(21), the only nonzero contributions to the average are models which have a (lower) bin boundary at  $t$ . Assume  $t$  was at the lower bound of bin  $j$ , i.e. at  $t = k_{j-1} + 1$  (the  $\{k_m\}$  are inclusive upper bin boundaries, as defined above). Carrying out the integrals over the  $\{f_m\}$  yields:

$$P(L = t, \{\mathbf{z}^i\}, \{k_m\}|M, S) = \int_0^1 d\{f_m\} P(L = t | \{k_m\}, \{f_m\}, M, S) p(\{\mathbf{z}^i\}, \{f_m\}, \{k_m\}|M) = \int_0^S df_0 \dots \int_0^S df_{j-1} \int_S^1 df_j \int_0^1 df_{j+1} \dots \int_0^1 df_M p(\{\mathbf{z}^i\}, \{f_m\}, \{k_m\}|M) \quad (\text{B-13})$$

The integration boundaries in the last line of eqn.(B-13) are a consequence of our latency definition: all bins  $m < j$  will contribute to the integral only as long as  $f_m < S$ , hence the upper bound of their integrals is at  $S$ . Bin  $j$  contributes only if  $f_j \geq S$ , thus the lower bound of the integral over  $f_j$  is  $S$ . The bins  $m > j$  are not affected by the latency probability (eqn.(21)) whence their integrals still run from 0 to 1. By virtue of eqn.(3) and eqn.(5), we obtain

$$P(L = t, \{\mathbf{z}^i\}, \{k_m\}|M, S) = \prod_{m=0}^{j-1} B_S(s(\{\mathbf{z}^i\}, m) + \sigma_m, g(\{\mathbf{z}^i\}, m) + \gamma_m) \times \bar{B}_S(s(\{\mathbf{z}^i\}, j) + \sigma_m, g(\{\mathbf{z}^i\}, j) + \gamma_m) \times \prod_{m=j+1}^M B(s(\{\mathbf{z}^i\}, m) + \sigma_m, g(\{\mathbf{z}^i\}, m) + \gamma_m) \times \prod_{m=0}^M \frac{1}{B(\sigma_m, \gamma_m)} P(\{k_m\}|M) \quad (\text{B-14})$$

where  $B_S(a, b) = \int_0^S t^{a-1} (1-t)^{b-1} dt$  is the incomplete Beta function (Davis 1972) and  $\bar{B}_S(a, b) = \int_S^1 t^{a-1} (1-t)^{b-1} dt = B(a, b) - B_S(a, b)$

is its complement. Note that up to the factor  $P(\{k_m\}|M)$ , eqn.(B-14) is basically eqn.(A-5) with some of the Beta functions replaced by incomplete Beta functions. Hence, the remaining summations over the  $\{k_m\}$  can be carried out by using

$$\begin{aligned} \text{getIEC}_L(k_s, k_e, m) &:= \\ &= \begin{cases} B_S(s(\{\mathbf{z}^i\}, k_s, k_e) + \sigma_m, g(\{\mathbf{z}^i\}, k_s, k_e) + \gamma_m) & \text{if } k_e < t \\ \tilde{B}_S(s(\{\mathbf{z}^i\}, k_s, k_e) + \sigma_m, g(\{\mathbf{z}^i\}, k_s, k_e) + \gamma_m) & \text{if } k_s = t \\ B(s(\{\mathbf{z}^i\}, k_s, k_e) + \sigma_m, g(\{\mathbf{z}^i\}, k_s, k_e) + \gamma_m) & \text{if } k_s > t \\ 0 & \text{otherwise} \end{cases} \quad (\text{B-15}) \end{aligned}$$

instead of  $\text{getIEC}(k_s, k_e, m)$  (eqn.(A-6)) in the evidence computation algorithm. This procedure yields the desired  $P(L = t, \{\mathbf{z}^i\}|M, S)$ . The above derivation is an instance of the general framework for computing expectations of functions of bin boundaries and firing probabilities described in (Endres and Földiák 2005).

### Appendix C: Computing the posterior density of the firing rate

We compute the joint probability density of the firing rate  $f(t) = \tilde{f}$ , the latency  $L = t$  and the observed spiketrains  $\{\mathbf{z}^i\}$  given the number of bins and the signal separation level  $S$  via

$$\begin{aligned} P(f(t) = \tilde{f}, L = t, \{\mathbf{z}^i\}|M, S) &= \\ &= \sum_{k_{M-1}=M-1}^{T-2} \sum_{k_{M-2}=M-2}^{k_{M-1}-1} \dots \sum_{k_0=0}^{k_1-1} P(f(t) = \tilde{f}, L = t, \{\mathbf{z}^i\}, \{k_m\}|M, S) \end{aligned} \quad (\text{C-16})$$

where

$$\begin{aligned} p(f(t) = \tilde{f}, L = t, \{\mathbf{z}^i\}, \{k_m\}|M, S) &= \\ &= \int_0^1 d\{f_m\} P(f(t) = \tilde{f}, L = t | \{k_m\}, \{f_m\}, M, S) P(\{\mathbf{z}^i\}, \{f_m\}, \{k_m\}|M) \end{aligned} \quad (\text{C-17})$$

Note that  $P(f(t) = \tilde{f}, L = t | \{k_m\}, \{f_m\}, M, S)$  is the r.h.s. of eqn.(24) and  $p(\{\mathbf{z}^i\}, \{f_m\}, \{k_m\}|M)$  is the numerator of the r.h.s. of eqn.(8). As a consequence of eqn.(24), the only nonzero contributions to the average are models which have a (lower) bin boundary at  $t$ . Assume  $t$  was at the lower bound of bin  $j$ , i.e. at  $t = k_{j-1} + 1$  (the  $\{k_m\}$  are inclusive upper bin boundaries, as defined above). Integrating out the  $\{f_m\}$  yields

$$\begin{aligned} p(f(t) = \tilde{f}, L = t, \{\mathbf{z}^i\}, \{k_m\}|M, S) &= \\ &= \prod_{m=0}^{j-1} B_S(s(\{\mathbf{z}^i\}, m) + \sigma_m, g(\{\mathbf{z}^i\}, m) + \gamma_m) \\ &\times \tilde{f}^{s(\{\mathbf{z}^i\}, j) + \sigma_m - 1} (1 - \tilde{f})^{g(\{\mathbf{z}^i\}, j) + \gamma_m - 1} \\ &\times \prod_{m=j+1}^M B(s(\{\mathbf{z}^i\}, m) + \sigma_m, g(\{\mathbf{z}^i\}, m) + \gamma_m) \\ &\times \prod_{m=0}^M \frac{1}{B(\sigma_m, \gamma_m)} P(\{k_m\}|M) \end{aligned} \quad (\text{C-18})$$

where the second line is a result of eqn.(3) and eqn.(5) multiplied with the Dirac delta function in eqn.(23). Hence, the remaining summations over the  $\{k_m\}$  can be carried out by using

$$\begin{aligned} \text{getIEC}_{f,L}(k_s, k_e, m) &:= \\ &= \begin{cases} B_S(s(\{\mathbf{z}^i\}, k_s, k_e) + \sigma_m, g(\{\mathbf{z}^i\}, k_s, k_e) + \gamma_m) & \text{if } k_e < t \\ \tilde{f}^{s(\{\mathbf{z}^i\}, k_s, k_e) + \sigma_m - 1} (1 - \tilde{f})^{g(\{\mathbf{z}^i\}, k_s, k_e) + \gamma_m - 1} & \text{if } k_s = t \\ B(s(\{\mathbf{z}^i\}, k_s, k_e) + \sigma_m, g(\{\mathbf{z}^i\}, k_s, k_e) + \gamma_m) & \text{if } k_s > t \\ 0 & \text{otherwise} \end{cases} \quad (\text{C-19}) \end{aligned}$$

instead of  $\text{getIEC}(k_s, k_e, m)$  (eqn.(A-6)) in the evidence computation algorithm. Thus we obtain  $P(f(t) = \tilde{f}, L = t, \{\mathbf{z}^i\}|M, S)$ .

### References

- Alitto HJ, Usrey WM (2004) Influence of contrast on orientation and temporal frequency tuning in ferret primary visual cortex. *Journal of Neurophysiology* 91:2797–2808
- Barracough N, Xiao D, Baker C, Oram M, Perrett D (2005) Integration of visual and auditory information by superior temporal sulcus neurons responsive to the sight of actions. *Journal of Cognitive Neuroscience* 17
- Berenyi A, Benedek G, Nagy A (2007) Double sliding-window technique: A new method to calculate the neuronal response onset latency. *Brain Research* 1178:141–148
- Berger J (1985) *Statistical Decision Theory and Bayesian Analysis*. Springer, New York
- Bertsekas DP (2000) *Dynamic Programming and Optimal Control*. Athena Scientific
- Cover T, Thomas J (1991) *Elements of Information Theory*. Wiley, New York
- Cunningham J, Yu B, Shenoy K, Sahani M (2008) Inferring neural firing rates from spike trains using Gaussian processes. In: Platt J, Koller D, Singer Y, Roweis S (eds) *Advances in Neural Information Processing Systems 20*, MIT Press, Cambridge, MA
- Davis P (1972) Gamma function and related functions. In: Abramowitz M, Stegun I (eds) *Handbook of mathematical functions*, Dover, New York
- DiMatteo I, Genovesi CR, E KR (2001) Bayesian curve-fitting with free-knot splines. *Biometrika* 88(4):1055–1071
- Edwards R, Xiao D, Keyzers C, Földiák P, Perrett DI (2003) Color Sensitivity of Cells Responsive to Complex Stimuli in the Temporal Cortex. *Journal of Neurophysiology* 90(2):1245–1256, DOI 10.1152/jn.00524.2002, URL <http://jn.physiology.org/cgi/content/abstract/90/2/1245>, <http://jn.physiology.org/cgi/reprint/90/2/1245.pdf>
- Eifuku S, De Souza WC, Tamura R, H N, T O (2004) Neuronal correlates of face identification in the monkey anterior temporal cortical areas. *Journal of Neurophysiology* 91:358–371
- Endres D (2006) Bayesian and information-theoretic tools for neuroscience. PhD thesis, School of Psychology, University of St. Andrews, U.K., <http://hdl.handle.net/10023/162>
- Endres D, Földiák P (2005) Bayesian bin distribution inference and mutual information. *IEEE Transactions on Information Theory* 51(11)
- Endres D, Oram M, Schindelin J, Földiák P (2008) Bayesian binning beats approximate alternatives: estimating peri-stimulus time histograms. In: Platt J, Koller D, Singer Y, Roweis S (eds) *Advances in Neural Information Processing Systems 20*, MIT Press, Cambridge, MA
- Földiák P, Xiao D, Keyzers C, Edwards R, Perrett DI (2004) Rapid serial visual presentation for the determination of neural selectivity in area STSa. *Progress in Brain Research* 144:107–116
- Friedman HS, Priebe CE (1998) Estimating stimulus response latency. *Journal of Neuroscience Methods* 83:185–194
- Fries P, Neunenschwander S, Engel AK, Goebel R, Singer W (2001) Rapid feature selective neuronal synchronization through correlated latency shifting. *Nature Neuroscience* 4:194–200
- Gabel SF, Misslislich H, Schaafsma SJ, Duysens J (2002) Temporal properties of optic flow responses in the ventral intraparietal area. *Visual Neuroscience* 19:381–388
- Gawne TJ, Kjaer TW, Hertz JA, Richmond BJ (1996a) Adjacent visual cortical complex cells share about 20% of their stimulus-related information. *Cerebral Cortex* 6(3):482–9
- Gawne TJ, Kjaer TW, Richmond BJ (1996b) Latency: another potential code for feature binding in striate cortex. *Journal of Neurophysiology* 76:1356–1360
- Hanes DP, Thompson KG, Schall JD (1995) Relationship of presaccadic activity in frontal eye field and supplementary eye field to

- saccade initiation in macaque - poisson spike train analysis. *Experimental Brain Research* 103:85–96
- Heil P, Irvine DRF (1997) First-spike timing of auditory-nerve fibers and comparison with auditory cortex. *Journal of Neurophysiology* 78:2438–2454
- Hurley LM, Pollak GD (2005) Serotonin shifts first-spike latencies of inferior colliculus neurons. *Journal of Neuroscience* 25:7876–7886
- Hutter M (2006) Bayesian regression of piecewise constant functions. Tech. Rep. arXiv:math/0606315v1, IDSIA-14-05
- Hutter M (2007) Exact bayesian regression of piecewise constant functions. *Journal of Bayesian Analysis* 2(4):635–664
- Kiani R, Esteky H, Tanaka K (2005) Differences in Onset Latency of Macaque Inferotemporal Neural Responses to Primate and Non-Primate Faces. *Journal of Neurophysiology* 94(2):1587–1596, DOI 10.1152/jn.00540.2004, URL <http://jn.physiology.org/cgi/content/abstract/94/2/1587>, <http://jn.physiology.org/cgi/reprint/94/2/1587.pdf>
- Lee J, Williford T, Maunsell JHR (2007) Spatial attention and the latency of neuronal responses in macaque area V4. *Journal of Neuroscience* 27:9632–9637
- Liu Z, Richmond BJ (2000) Response differences in monkey te and perirhinal cortex: Stimulus association related to reward schedules. *Journal of Neurophysiology* 83:1677–1692
- Loader C (1997) LOCFIT: an introduction. *Statistical Computing and Graphics Newsletter* 8(1):11–17, uRL: <http://www.stat-computing.org/newsletter>
- Loader C (1999) *Local Regression and Likelihood*. Springer, New York
- Luczak A, Bartho P, Marguet SL, Buzsaki G, Harris KD (2007) Sequential structure of neocortical spontaneous activity in vivo. *Proceedings of the National Academy of Sciences USA* 104:347–352
- Maunsell JH, Gibson JR (1992) Visual response latencies in striate cortex of the macaque monkey. *Journal of Neurophysiology* 68:1332–1344
- Nawrot MP, Aertsen A, Rotter S (2003) Elimination of response latency variability in neuronal spike trains. *Biological Cybernetics* 88:321–334
- Nemenman I, Bialek W, van Steveninck R (2004) Entropy and information in neural spike trains: Progress on the sampling problem. *Physical Review E* 69(5):056111, URL <http://link.aps.org/abstract/PRE/v69/e056111>
- Nowak LG, Munk MHJ, Girard P, Bullier J (1995) Visual latencies in areas v1 and v2 of the macaque monkey. *Visual Neuroscience* 12:371–384
- Optican L, Gawne T, Richmond B, Joseph P (1991) Unbiased measures of transmitted information and channel capacity from multivariate neuronal data. *Biological Cybernetics* 65:305–310
- Oram M, Perret D (1996) Integration of form and motion in the anterior superior temporal polysensory area (stpa) of the macaque monkey. *Journal of Neurophysiology* 19:109–129
- Oram MW, Perrett DI (1992) Time course of neural responses discriminating different views of the face and head. *Journal of Neurophysiology* 68(1):70–84
- Oram MW, Xiao D, Dritschel B, Payne K (2002) The temporal precision of neural signals: A unique role for response latency? *Philosophical Transactions of the Royal Society, Series B* 357:987–1001
- Paninski L (2004) Estimating entropy on m bins given fewer than m samples. *IEEE Transactions on Information Theory* 50(9):2200–2203
- Panzeri S, Treves A (1996) Analytical estimates of limited sampling biases in different information measures. *Network: Computation in Neural Systems* 7:87–107
- Perrett DI, Oram MW, Harries MH, Bevan R, Hietanen JK, Benson PJ (1991) Viewer-centered and object-centered coding of heads in the macaque temporal cortex. *Experimental Brain Research* 86:159–173
- Press W, Flannery B, Teukolsky S, Vetterling W (1986) *Numerical Recipes in C: The Art of Scientific Computing*. Cambridge University Press, New York
- Richmond BJ, Optican LM (1987a) Temporal encoding of two-dimensional patterns by single units in primate inferior temporal cortex. ii. quantification of response waveform. *Journal of Neurophysiology* 57(1):147–161
- Richmond BJ, Optican LM (1987b) Temporal encoding of two-dimensional patterns by single units in primate inferior temporal cortex. iii. information theoretic analysis. *Journal of Neurophysiology* 57(1):162–178
- Richmond BJ, Oram MW, Wiener MC (1999) Response features determining spike times. *Neural Plasticity* 6:133–145
- van Rossum MCW, van der Meer MAA, Xiao D, Oram MW (2008) Adaptive Integration in the Visual Cortex by Depressing Recurrent Cortical Circuits. *Neural Computation* 20(7):1847–1872, URL <http://neco.mitpress.org/cgi/content/abstract/20/7/1847>, <http://neco.mitpress.org/cgi/reprint/20/7/1847.pdf>
- Sary G, Koteles K, Chadaide Z, Tompa T, Benedek G (2006) Task-related modulation in the monkey inferotemporal cortex. *Brain Research* 1121:76–82
- Schmoleky MT, Wang Y, Hanes DP, Thompson KG, Leutgeb S, Schall JD, Leventhal AG (2006) Signal timing across the macaque visual system. *Journal of Neurophysiology* 95:3272–3278
- Shannon CE (1948) The mathematical theory of communication. *The Bell Systems Technical Journal* 27:379–423, 623–656
- Shimazaki H, Shinomoto S (2007a) Kernel width optimization in the spike-rate estimation. In: Budelli R, Caputi A, Gomez L (eds) *Neural Coding 2007*, pp 143–146, URL <http://neuralcoding2007.edu.yu>
- Shimazaki H, Shinomoto S (2007b) A method for selecting the bin size of a time histogram. *Neural Computation* 19(6):1503–1527
- Shimazaki H, Shinomoto S (2007c) A recipe for optimizing a time-histogram. In: Schölkopf B, Platt J, Hoffman T (eds) *Advances in Neural Information Processing Systems 19*, MIT Press, Cambridge, MA, pp 1289–1296
- Shinomoto S, Koyama S (2007) A solution to the controversy between rate and temporal coding. *Statistics in Medicine* 26:4032–4038
- Stecker GC, Middlebrooks JC (2003) Distributed coding of sound locations in the auditory cortex. *Biological Cybernetics* 89:341–349
- Sugase-Miyamoto Y, Richmond BJ (2005) Neuronal signals in the monkey basolateral amygdala during reward schedules. *Journal of Neuroscience* 25:11,071–11,083
- Syka J, Popelar J, Kvasnak E, Astl J (2000) Response properties of neurons in the central nucleus and external dorsal cortices of the inferior colliculus in guinea pig. *Experimental Brain Research* 133:254–266
- Tamura H, Tanaka K (2001) Visual response properties of cells in the ventral and dorsal parts of the macaque inferotemporal cortex. *Cerebral Cortex* 11:384–399
- Tanaka M, Lisberger SG (2002) Role of arcuate frontal cortex of monkeys in smooth pursuit eye movements. I. Basic response properties to retinal image motion and position. *Journal of Neurophysiology* 87:2684–2699
- Thompson KG, Hanes DP, Bichot NP, Schall JD (1996) Perceptual and motor processing stages identified in the activity of macaque frontal eye field neurons during visual search. *Journal of Neurophysiology* 76:4040–4055
- Tovee MJ, Rolls ET, Treves A, Bellis RP (1993) Information encoding and the responses of single neurons in the primate temporal visual cortex. *Journal of Neurophysiology* 70(2):640–654, URL <http://jn.physiology.org/cgi/content/abstract/70/2/640>, <http://jn.physiology.org/cgi/reprint/70/2/640.pdf>

Ventura V (2004) Testing for and estimating latency effects for poisson and non-poisson spike trains. *Neural Computation* 16(11):2323–2349, DOI <http://dx.doi.org/10.1162/0899766041941952>